TECHNISCHE
UNIVERSITÄT
WIEN

Diploma Thesis

Design and construction of an acetylene capable PVD based deposition system

by

Stefan Rißlegger

Mat. Nr.: 0430468

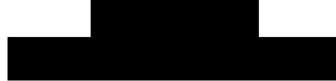

carried out for the purpose of obtaining the degree Master of Science

under the supervision of

Univ.Prof. Dipl.-Ing. Dr.mont. Paul Heinz Mayrhofer

Univ.Ass. Dipl.-Ing. Dr.techn. Helmut Riedl-Tragenreif

Institute of Materials Science and Technology – E308

Materials Science Division

submitted at

Faculty of Mechanical and Industrial Engineering

TU Wien

Vienna, 27th of March, 2020

Die approbierte gedruckte Originalversion dieser Diplomarbeit ist an der TU Wien Bibliothek verfügbar
The approved original version of this thesis is available in print at TU Wien Bibliothek.
TU WIEN Bibliothek Your knowledge hub

Die approbierte gedruckte Originalversion dieser Diplomarbeit ist an der TU Wien Bibliothek verfügbar
The approved original version of this thesis is available in print at TU Wien Bibliothek.
TU Bibliothek Your knowledge hub WIEN

“... in Wirklichkeit gibt es nur Atome im leeren Raum.“

– Demokrit (460-370 B.C.)

This work was supported by Plansee Composite Materials GmbH and Oerlikon Balzers, Surface Solutions AG in the framework of the Christian Doppler Laboratory for Surface Engineering of High-Performance Components as well as the Christian Doppler Laboratory for Application Oriented Coating Development.

Affidavit:

I declare in lieu of oath, that I wrote this thesis and performed the associated research myself, using only literature cited in this volume.

Date	Signature

Die approbierte gedruckte Originalversion dieser Diplomarbeit ist an der TU Wien Bibliothek verfügbar
The approved original version of this thesis is available in print at TU Wien Bibliothek.
TU WIEN Bibliothek Your knowledge hub

Die approbierte gedruckte Originalversion dieser Diplomarbeit ist an der TU Wien Bibliothek verfügbar
The approved original version of this thesis is available in print at TU Wien Bibliothek.
TU WIEN Bibliothek Your knowledge hub

Acknowledgements

First of all, I would like to thank my supervisor **Paul H. Mayrhofer** for welcoming me into his research group and making this thesis possible. His commitment and positive attitude make the working group an amazing team. Even though you have innumerable functions, it seems that you always have time for your flock. Thanks, Paul.

Furthermore, I am very thankful to have been supervised by **Helmut Riedl-Tragenreif**. His motivation to always enhance systems and labs to improve research requirements often presented me with challenging, but always exciting tasks. At the same time, he always had an open ear for the most diverse concerns. Helmut, I would like to thank you for your commitment during my thesis and in the group and wish you good luck for your future.

My colleague and friend **Philipp Ertelthaler** made an important and major contribution to this work. He introduced me to the world of PVD systems and was a good mentor at all times, both in technical and sometimes in human matters. I am glad to have had many discussions and exchanges with you. Philip, I hope that our paths never get lost.

Special thanks also go to **Thomas Glechner**, who acted as test pilot and will continue to look after Frida in the future. I wish you much success and fun with the little lady.

A further thank you goes to all my other colleagues, especially those who have contributed with a helping hand during the construction or with expert discussions. It was a honor for me to work with **Alex K, Alex S, Antonia, Arnold, Christian, Christoph, David, Elias, Julian, Lorenz, Lukas L., Lukas Z., Matthias, Nikola, Oliver, Philipp K., Rainer, Stefan G., Stefan K., Tom, Valentin, Veit, Vincent** and many more. I got to know you as colleagues and am happy to call many of you now as friends, bros, the gang or even wingman. You were responsible for a good time. I wish you all continued success and that your spirit and humor remain.

Last but not least I would like to thank my **family** and **friends**. Your support and your presence have always helped me to find and follow my way. Thank you for every uplifting word, and the good moments. It is wonderful to have you by my side or behind me.

Table of Contents

Table of Contents i

List of Symbols & Abbreviations iii

Abstract vii

1 Introduction 1

2 Vacuum Technology 3

2.1 Gas laws and rarefied gas flow 3

2.2 Materials for Vacuum Applications 8

2.2.1 Metals 8

2.2.2 Glasses and Ceramics 10

2.2.3 Polymers 10

2.3 Vacuum Pumps 12

2.3.1 Rotary vane pumps 14

2.3.2 Diaphragm pumps 16

2.3.3 Screw pumps 16

2.3.4 Roots pumps 18

2.3.5 Claw pumps 19

2.3.6 Turbomolecular pumps 20

2.4 Vacuum Pressure Analysis 22

2.4.1 Capacitive diaphragm vacuum manometers 22

2.4.2 Piezo vacuum gauges 23

2.4.3 Pirani vacuum gauges 23

2.4.4 Cathode ionization vacuum gauges 24

Die approbierte gedruckte Originalversion dieser Diplomarbeit ist an der TU Wien Bibliothek verfügbar
The approved original version of this thesis is available in print at TU Wien Bibliothek.
TU WIEN Bibliothek Your knowledge hub

3 Physical Vapor Deposition 26
3.1 Sputtering 27
3.2 Reactive Magnetron Sputtering 29
3.3 Film Growth 31
4 Diamond-Like Carbon 33
5 Design of the PVD System ”Frida” 36
5.1 Vacuum and Chamber Design 38
5.2 Gas Distribution 42
5.3 Electrical design and safety 47
5.3.1 General structure 47
5.3.2 Safety 47
5.4 Substrate handling 50
5.5 Magnetron 54
5.6 Machine frame and cooling water 55
5.7 Operation 57
5.8 Outlook 59
6 List of Figures 60
7 List of Tables 62
8 References 63
A. Objects I
B. Temperature Calibration Curves III
C. Figure V

Die approbierte gedruckte Originalversion dieser Diplomarbeit ist an der TU Wien Bibliothek verfügbar
The approved original version of this thesis is available in print at TU Wien Bibliothek.
TU WIEN Bibliothek Your knowledge hub

List of Symbols & Abbreviations

A .... Area

B'' .... Second Virial coefficient

C_R .... Backflow conductivity

E^* .... Normalized energy

E_I .... Kinetic energy of the ion

E_{th} .... Threshold energy

F .... Force

F_p .... Force of the particle

K .... Compression ratio

Kn .... Knudsen number

M .... Molar mass

M_I .... Mass of the ion

M_T .... Mass of the sputtered target atom

N .... Particle Number

N_A .... Avogadro´s number

Q_{des} .... Desorption rate

Q_{diff} .... Diffusion rate

Q_L .... Leak rate

Q_{perm} .... Permeation flow

R .... Molar gas constant

R_s .... Specific gas constant

S .... Pumping speed

S_{eff} .... Effective pumping speed

TU WIEN Bibliothek Your knowledge hub
Die approbierte gedruckte Originalversion dieser Diplomarbeit ist an der TU Wien Bibliothek verfügbar
The approved original version of this thesis is available in print at TU Wien Bibliothek.

T .... Temperature

T^* .... Generalized temperature

T_h .... Homologous temperature

T_m .... Melting temperature

U_S .... Binding energy of surface atom

V .... Volume

Y .... Sputter yield

α .... Thermal expansion coefficient, angle

λ .... Wave length, mean free path

ν .... Particle number density

a .... Van der Waals parameter

b .... Van der Waals parameter

c .... Speed

$\bar{c}$ .... Arithmetic mean thermal speed

c_x .... Velocity

d .... Length, diameter

g .... Factor of free path to wall

k .... Boltzmann´s constant

k_{perm} .... Permeation constant

m .... Mass

m_p .... Mass of the particle

n .... Amount of substance

n_2 .... Density of discharge gas

p .... Pressure

p_a .... External pressure

p_i .... Partial pressure

p_p .... Pressure of the particle

q_{des} .... Specific desorption rate

q_{diff} .... Specific diffusion density

Die approbierte gedruckte Originalversion dieser Diplomarbeit ist an der TU Wien Bibliothek verfügbar
The approved original version of this thesis is available in print at TU Wien Bibliothek.
TU WIEN Bibliothek Your knowledge hub

q_{pV} .... Throughput

r_1, r_2 .... Atomistic radii

t .... Time

t^* .... Thickness of layer

u .... Circumferential speed

AC .... Alternating current

ALD .... Atomic layer deposition

CAD .... Computer aided design

CMR .... Capacitive diaphragm vacuum gauge

COF .... Coefficient of friction

CVD .... Chemical vapor deposition

DC .... Direct current

DLC .... Diamond like carbon

EPDM .... Ethylene propylene diene monomer rubber

FKM .... Fluoroelastomer

FPM .... Fluoroelastomer

HiPIMS .... High power impulse magnetron sputtering

HV .... High vacuum

IKR .... Cold cathode vacuum gauge

Me .... Metal

MF .... Mid frequency

MFC .... Mass flow controller

OFHC .... Oxygen free high conductive

PACVD .... Plasma assisted chemical vapor deposition

PECVD .... Plasma enhanced chemical vapor deposition

PCR .... Pirani capacitive diaphragm vacuum gauge

PEEK .... Polyether ether ketone

POM .... Polyoxymethylene

Die approbierte gedruckte Originalversion dieser Diplomarbeit ist an der TU Wien Bibliothek verfügbar
The approved original version of this thesis is available in print at TU Wien Bibliothek.
TU WIEN Bibliothek Your knowledge hub

PTFE..Polytetrafluorethylene

PVD..Physical vapor deposition

SIL..Safety integrity level

SZD..Structure zone diagram

UHV..Ultra high vacuum

VS..Vacuum switch

a..amorphous

ta..tetrahedral amorphous

Die approbierte gedruckte Originalversion dieser Diplomarbeit ist an der TU Wien Bibliothek verfügbar
The approved original version of this thesis is available in print at TU Wien Bibliothek.
TU Wien Bibliothek Your knowledge hub

Abstract

In the field of hard materials, and especially hard coatings, are carbon-based compounds one of the most important and prevalent material class being still topic of diverse research activities. Since the discovery and commercialization of cemented carbides in the early 1920's – e.g. the alloy WIDIA (in German: "Wie Diamant") implying the term diamond like – the variety of carbon-based alloys and coating materials increased vastly. The properties that come close to those of diamonds have inspired scientists and engineers worldwide for decades. In particular, the synthesis of diamond-like carbon (DLC) coatings using the full variety of physical vapor deposition techniques is still an ongoing challenge.

The impressive track record of DLC based coatings, is not only related to the unique tribo-mechanical properties – hardness between 60 to 80 GPa (highly pure diamonds obtain 100 GPa or even higher) combined with coefficient of frictions (COF) below 0.05 – but also to the well-described characterization and synthesis methods. Especially, the broad range of bonding states, e.g. tetrahedral amorphous carbon (ta-C) or amorphous carbon with or without metal constituents (a-C or a-C:Me), accessible by sputtering is a key-factor of this deposition technique. Nevertheless, the application of reactive gases – such as acetylene (C_2H_2) – during sputter deposition also implies the introduction of hydrogen and hence a drastic change of the coating properties – especially, reduced hardness for ta:C:H based coatings. Recent studies highlighted that a pronounced ionization of acetylene during sputtering results in a larger proportion of sp^3 hybridized carbon and hence increased hardness values.

High Power Impulse Magnetron Sputtering (HiPIMS) is one possibility to control the ionization state of metal but also non-metal species during reactive sputter deposition. However, these processes have not yet been fully described by academia as well as industrial application on large scale facilities are still pending. One strong limitation is the lack of available lab-scale sputter deposition systems simultaneously capable for acetylene and HiPIMS. Therefore, the aim of this thesis is to design and construct a lab-scale PVD system contributing to future research in the field of carbon-based coating materials by reactive HiPIMS – getting even closer to unreached coating properties.

TU WIEN Bibliothek Your knowledge hub
Die approbierte gedruckte Originalversion dieser Diplomarbeit ist an der TU Wien Bibliothek verfügbar
The approved original version of this thesis is available in print at TU Wien Bibliothek.

1 Introduction

Since the industrial revolution in the 19th century, technological progress has almost always been linked to the further development of materials. For more than a century, surface technology has made a significant contribution in protecting and improving bulk materials. Physical vapor deposition (PVD) has been used for over eight decades to extend the life and performance of components. Since the 1960s, carbon layers, later called diamond like carbon (DLC), have been researched. At about the same time sputtering and later magnetron sputtering became well established.

For more than 20 years, DLC coatings have been manufactured industrially and can be found on today's daily used consumer goods such as razor blades or car parts. The high hardness and the low coefficient of friction (COF) are the main reasons to apply these coatings to components. A negative effect of the high compressive stresses of the coatings, which have in turn a positive impact on the hardness, is the poor coating adhesion. In addition to adhesive interlayers, metal-containing DLC coatings have also been developed to solve this problem. Mainly amorphous hydrogenated (a-C:H:Me) layers with high hydrogen content are well investigated, which contain a high percentage of sp^2 bonded carbon and therefore have lower hardness. Super hard layers on the other hand have a high fraction of sp^3 hybridized carbon. These hydrogen-free tetrahedral amorphous carbon layers (ta-C) reach hardness values of almost 80 GPa. In addition to cathodic arc evaporated and laser arced coatings, high sp^3 fractions are achieved with pulsed laser deposition and unbalanced magnetron sputtering. Especially a high ionization rate and the application of appropriate bias voltage have shown promising results according to a number of research works with unbalanced magnetron sputtering [1].

Research also shows how hydrocarbons as a precursor gas can be used to improve the coating properties and make new applications possible. Especially acetylene with its high C/H ratio is very interesting and suitable for the generation of highly sp^3 hybridized layers. The technology for the deposition of super hard ta:C layers is still not sufficiently researched and used full industrially. High power impulse magnetron sputtering (HiPIMS) with acetylene as

Die approbierte gedruckte Originalversion dieser Diplomarbeit ist an der TU Wien Bibliothek verfügbar
The approved original version of this thesis is available in print at TU Wien Bibliothek.
TU Bibliothek WIEN Your knowledge hub

reactive gas is one of the promising possibilities to produce hard DLC coatings with lowest COF [2, 3].

Adequate coating equipment is necessary to further research. Especially the use of small research facilities offers advantages in terms of adaptability and simple, fast and cost-effective operation. For example, it is easier to produce small targets from novel materials made of brittle ceramic carbons. In addition, developments and changing requirements can be responded to more quickly for small systems. Unfortunately, there are hardly any lab-scale plants available which can be operated with acetylene as reactive gas. For this purpose, the system described in this thesis was developed and built to provide the necessary basis for the experimental investigations of DLC and transition metal carbides in the Thin Films Materials Science division of the TU Wien.

Die approbierte gedruckte Originalversion dieser Diplomarbeit ist an der TU Wien Bibliothek verfügbar
The approved original version of this thesis is available in print at TU Wien Bibliothek.
TU WIEN Bibliothek Your knowledge hub

2 Vacuum Technology

Vacuum technology is one of the basic requirements in many different fields of industry and science – ranging from simple food packing, to cleaning techniques, or medical applications, up to micro-electronics and further nano-technologies. Especially, for surface engineering vacuum science is essential as most of the well-known deposition techniques – such as atomic layer deposition (ALD), chemical vapor deposition (CVD), or physical vapor deposition (PVD) techniques – require well-defined vacuum conditions. At the outset of every deposition process a proper base pressure is a prerequisite to synthesis high-quality coating materials. Here, the leakage and reliability of vacuum chambers and gas supplies are crucial. Therefore, it is necessary to fundamentally understand the physics of rarefied gas, vacuum generation technique as well as vacuum pressure analysis. Within this chapter all important considerations are taken into account.

2.1 Gas laws and rarefied gas flow

Vacuum is defined as a state of gas in a vessel with a pressure below the surrounding atmosphere. More detailed, a pressure below 300 mbar according to DIN 28400-1 [4] is termed as a vacuum pressure. In contrast to many other fields, e.g. hydraulics, the absolute pressure is meant and refers to an ideal vacuum, which in turn is defined as a volume or 3D space without any particles (specifically molecules and atoms). The pressure (p) is defined as the ratio of the force (F) perpendicular on a surface with the area (A), see Equation (2.1).

$$p \coloneqq \frac{F}{A} \tag{2.1}$$

To describe thermodynamic systems, the amount of the substance is also essential. Usually the mass (m), particle number (N) or the amount of substance (n) is used. Especially vacuum and PVD systems are described with the latter two, due to the physical character. They are related via the Avogadro's number, $N_A = 6.02214076 \cdot 10^{23}$ mol^{-1}, see Equation (2.2). The second important intensive state variable is the thermodynamic temperature (T) in Kelvin [K]. As the amount of a substance is defined for a volume (V), this brings us to the equation of

Die approbierte gedruckte Originalversion dieser Diplomarbeit ist an der TU Wien Bibliothek verfügbar
The approved original version of this thesis is available in print at TU Wien Bibliothek.
TU WIEN Bibliothek Your knowledge hub

state for an ideal gas (Equation 2.3). R is the molar gas constant and is calculated with N_A and Boltzmann's constant, $k = 1.380649 \cdot 10^{-23}$ J K^{-1}. R_s is the specific gas constant, whereas M refers to the molar mass (see Equation 2.4).

$$n = \frac{N}{N_A} \tag{2.2}$$

$$p \cdot V = n \cdot R \cdot T = N \cdot k \cdot T \tag{2.3}$$

$$R = N_A \cdot k = 8.314462618 \text{ J mol}^{-1}\text{K}^{-1} \quad \text{and} \quad R_s = \frac{R}{M} = \frac{k}{m_p} \tag{2.4}$$

Equation (2.3) is sufficient for many considerations under standard conditions. To describe mixtures of different gas species the partial pressure (p_i) will be introduced at this point. It can be understood as the prevailing pressure of the same amount of one gas species alone present in the same total volume. The sum of p_i gives the total pressure according Equation (2.5) [5].

$$p = \sum_i p_i \tag{2.5}$$

Gases are able to transmit frictional forces and thermal energy, and influences diffusion. To describe these properties of gases, a macroscopic approach is used. Kinetic gas theory outlines the interaction between atoms and molecules and the surrounding walls due to their thermal movement. If ideally elastic collisions are assumed, the total energy is maintained, but the velocity and direction of the particles change, as in Newton's conservation of momentum. The pressure can now be expressed as the force of the impacting particles on a container wall (see Figure 2.1).

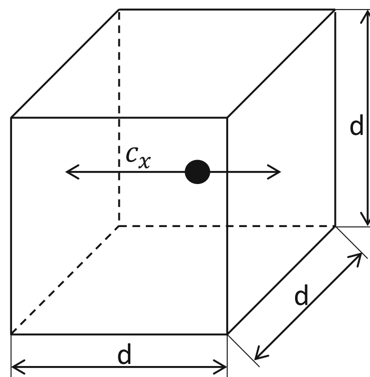

Fig. 2.1: Cube and particle movement to determine the pressure, adapted from [5].

Die approbierte gedruckte Originalversion dieser Diplomarbeit ist an der TU Wien Bibliothek verfügbar
The approved original version of this thesis is available in print at TU Wien Bibliothek.
TU WIEN Bibliothek Your knowledge hub

For this purpose, the molecules are assumed to be small hard spheres with a fixed diameter. Under these conditions, the viscosity, diffusion and thermal conductivity can also be described with sufficient accuracy for initial observations [5, 6].

A cube with side length (d) contains (N) particles with mass (m_p). The particle diameter is assumed to be negligibly small. The particles hit the wall with the constant velocity (c_x) and are elastically scattered in opposite directions. This corresponds to a momentum change of $m_p \cdot c_x$ and is endless repeated with a factor of $2d / c_x$. The force of a particle (F_p) can be expressed with the Equation (2.6), containing the resulting pressure (p_p) on a wall with the Equation (2.7).

$$F = m_p \cdot \frac{c_x^2}{d} \tag{2.6}$$

$$p_p = m_p \cdot \frac{c_x^2}{d^3} \tag{2.7}$$

The total pressure results now by multiplying the number of particles impinging on one wall (perpendicular to the x-axis) as follows:

$$p = \frac{N}{3}\, m_p \frac{c_x^2}{V} \quad \text{or} \quad p \cdot V = \frac{N}{3}\, m_p\, c_x^2 \tag{2.8}$$

If Equations (2.3) and (2.8) are assumed to be correct, Equation (2.9) applies to c_x and its absolute value – the speed (c) – which is equal in this model. An important conclusion of the equations is the temperature dependence of the particle velocity and thus the effect on the pressure.

$$c_x = c = \sqrt{\frac{3\,k\,T}{m_p}} = \sqrt{\frac{3\,R\,T}{M}} = \sqrt{3\,R_s\,T} \tag{2.9}$$

So far, we have assumed a constant velocity for all particles. In reality, however, it follows the Maxwell-Boltzmann velocity distribution, which resembles a bell-shaped Gaussian distribution. The arithmetic mean thermal speed ($\bar{c}$) is described:

$$\bar{c} = \sqrt{\frac{8\,k\,T}{\pi\,m_p}} = \sqrt{\frac{8\,R\,T}{\pi\,M}} = \sqrt{\frac{8}{\pi}\,R_s T} = \sqrt{\frac{8\,p}{\pi\,\rho}} \tag{2.10}$$

Furthermore, the mean free path (λ) is of crucial importance for vacuum- and specially PVD-technology. It is defined as the distance of a particle (sputtered atom) motion until a collision

Die approbierte gedruckte Originalversion dieser Diplomarbeit ist an der TU Wien Bibliothek verfügbar
The approved original version of this thesis is available in print at TU Wien Bibliothek.
TU Bibliothek WIEN Your knowledge hub

occurs. With a particle diameter (d) and the application of the Maxwell-Boltzmann distribution, λ results as follows:

$$\lambda = \frac{k\,T}{\sqrt{2}\;\pi\;\mathrm{d}^2\,p} \tag{2.11}$$

As the velocity of sputtered species is much larger than of gas molecules, Wasa [7] gives an estimation for λ where r_1 and r_2 are the atomic radii of sputtered atoms or gas molecules and n_2 is the density of discharge gas:

$$\lambda \cong \frac{1}{\pi\;(\mathrm{r}_1 + r_2)^{\,2} \cdot n_2} \tag{2.12}$$

At low pressures and correspondingly high λ, the interactions between particles due to collisions are very small. Due to this, the flow of gas in high vacuum regions can no longer be called viscous. Knudsen proved this so called molecular flow with experiments in 1909 [8]. Flow conditions in vacuum technology are nowadays described via the Knudsen number (Kn), see Equation (2.13), where d is the pipe diameter or rather the characteristic length. The physical behavior of gas flow can be distinguished using this value, which is inverse proportional to the pressure. Kn below 0.01 indicates viscous flow, $0.01 < Kn < 1$ is the transitional flow, with $Kn > 1$ molecular flow is meant. These boundaries vary in the literature, and are therefore not considered to be exact limits [5, 9].

$$Kn = \frac{\lambda}{d} \tag{2.13}$$

Table 2.1 shows common used limits for different vacuum ranges, with the particle number density $\nu = N/V$.

Die approbierte gedruckte Originalversion dieser Diplomarbeit ist an der TU Wien Bibliothek verfügbar
The approved original version of this thesis is available in print at TU Wien Bibliothek.
TU WIEN Bibliothek Your knowledge hub

Table 2.1: Pressure regimes and their characteristics, rounded to powers of tens [4, 5, 9].

Quantity	Symbol	Unit	Low vacuum (rough vacuum)	Medium vacuum (fine vacuum)	High vacuum (HV)	Ultra-high vacuum (UHV)
Pressure	p	Pa	10^5 – 100	100 – 0.1	0.1 - 10^{-5}	$<10^{-5}$
Particle number density	ν	cm^{-3}	10^{19} – 10^{16}	10^{16} – 10^{13}	10^{13} – 10^9	$<10^9$
Mean free path	λ	m	10^{-7} – 10^{-4}	10^{-4} – 0.1	0.1 – 10^3	$>10^3$
Flow regimes	-	-	Viscous flow	Transition flow	Molecular flow	Molecular flow

For most calculations in vacuum technology, the previous assumptions made with the ideal gas Equation (2.3) are sufficiently accurate [9]. Nevertheless, some more detailed calculation methods will be explained in the following. The attraction and repulsion forces of gas particles have not been considered so far. Van der Waals formulated the Equation (2.14) in 1873 where he included parameters for these effects on pressure. The parameters a and b now take the internal pressure and volume of the particles into account.

$$p = \frac{nRT}{V - nb} - \frac{n^2}{V^2}\, a \tag{2.14}$$

However, these parameters do not include temperature dependency, which leads to insufficiently accurate results, especially for the second term on the right side. A more precise approach therefore is the Virial Equation (2.15), here in the simplified form, terminated after the first order. B'' is the second virial coefficient [5, 10].

$$p = \frac{nRT}{V}\,(1 + B''(T)\,p) \tag{2.15}$$

Values for a, b and B'' can be found in literature, e.g. [5].

Die approbierte gedruckte Originalversion dieser Diplomarbeit ist an der TU Wien Bibliothek verfügbar
The approved original version of this thesis is available in print at TU Wien Bibliothek.
TU WIEN Bibliothek Your knowledge hub

2.2 Materials for Vacuum Applications

In vacuum technology, some specific requirements are placed on the materials used. Besides the mechanical properties, gas tightness and outgassing behavior are very important. Depending on the application, thermal resistance or thermal shock resistance, as well as electrical conductivity or dielectric strength are also required. The most important materials and their usage are described below.

2.2.1 Metals

Stainless steel is the most common used material in vacuum applications. However, it is also possible to use mild steel or more general structural steel. If there are no special requirements regarding corrosion or chemical resistance, these cost-effective materials can be used for HV regimes. On the other hand, the high carbon content and the contamination with phosphorus and sulfur can influence processes carried out within the vacuum system. For example, the constant release of CO can be a problem. Although in principle the weldability of unalloyed or low-alloy steels is well understood and manageable, the welding processes must be adapted for use in vacuum. Segregation must be avoided, as likewise hot cracks. The latter lead to so called latent or virtual leaks. This also applies to other metals suitable for welding. Mild steel can be used for magnetic shielding due to its high magnetic permeability [5].

A wide range of stainless steels offers good solutions for applications up to the UHV range. The strength is still sufficient even for thermally stressed components, e.g. baking processes up to 300 °C, which is important for flange joints. Stainless steels are corrosion resistant due to natural passivation at chromium contents of > 10.5 wt.% (typically >16 wt.%). The Cr_2O_3 layer is self-healing, therefore corrosion resistance is sufficient even in case of mechanical damage [6]. Depending on the alloying content, there are advantages and disadvantages in terms of processing and applications. EN 10088-1 defines stainless steels with C < 1.2 wt.% and Cr > 10.5 wt.% and lists the chemical compositions of the various stainless steel alloys [11]. Other important elements are Ni, Mo, Si, Mn, Al, Ti, Nb, N, V, Co and W. Figure 2.2 shows the most important stainless steels, the arrow points in the direction of the improved properties. The higher yield strength is usually achieved by increased nitrogen content or cold forming. The latter, however, has a negative effect on the often required low magnetisability. Furthermore, stainless steels have a low outgassing rate. This can be further improved by electrochemical polishing of the surface. Fine polishing or mirror polishing will

Die approbierte gedruckte Originalversion dieser Diplomarbeit ist an der TU Wien Bibliothek verfügbar
The approved original version of this thesis is available in print at TU Wien Bibliothek.
TU WIEN Bibliothek Your knowledge hub

further reduce the outgassing rate, but may not be applicable depending on the geometry. The positive effect is mainly due to the reduced surface area and the lower diffusion rate for adsorbing impurities during atmospheric conditions [12]. Geyari summarized the most important selection criteria for the use of stainless steels in vacuum applications [13].

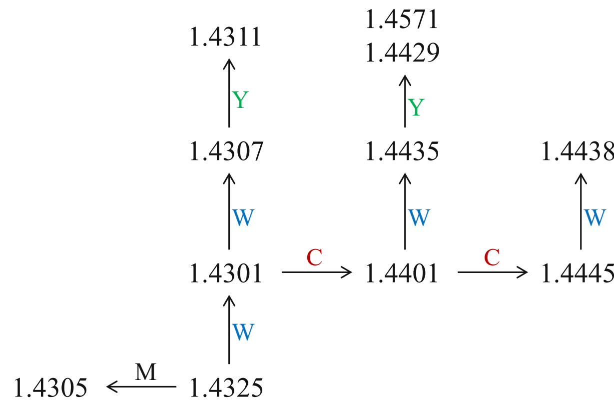

Fig. 2.2: Stainless steel in vacuum technology, C = corrosion resistance, M = machinability, W = weldability, Y = yield strength; adapted from [13].

The use of easily machinable stainless steels, such as 1.4305, should be avoided if possible, as these have an higher content of materials with high vapor pressure, e.g. S, P or Se [14]. If it is necessary to join flanges or other metallic components with glass or ceramics, thermal expansion can be a problem. This may lead to cracks in the application of conventional stainless steels, if they can be joined at all. Special alloys with a high nickel and cobalt content are used for this purpose. The alloy is composed of approximately 54 wt.% Fe, 29 wt.% Ni and 17 wt.% Co and is therefore called FerNiCo, better known as Kovar. However, these materials are in turn highly magnetic [5, 6].

Furthermore, aluminum is widely used in vacuum applications. It is easy to machine, but difficult to join with other metals. Connections to other components must be sealed with elastomers at atmospheric boundaries, such as flanges. Due to the low hardness of Al, conventional metal gaskets cannot be used. At a low melting temperature of about 660 °C, Al still has a relatively low vapor pressure of about 10^{-8} mbar.

In vacuum technology, copper is often used as a heat conductor, mostly for cooling purposes, or as an electrical conductor. To avoid so-called “hydrogen sickness” [15], oxygen-free high conductive (OFHC) copper is used. The most common use, however, is as a UHV seal for flanges, which can be baked to 450 °C [5].

TU Bibliothek Your knowledge hub WIEN
Die approbierte gedruckte Originalversion dieser Diplomarbeit ist an der TU Wien Bibliothek verfügbar
The approved original version of this thesis is available in print at TU Wien Bibliothek.

2.2.2 Glasses and Ceramics

Glass is widely used in vacuum technology because of its optical properties – as viewing window, beam entry or as a cover for heating elements due to the transmission of infrared radiation. In addition, the chemical resistance is excellent, which means that almost all corrosive media can be handled. Due to its amorphous structure it behaves differently to metals or other construction materials. The high brittleness and low tensile strength only allow limited use for mechanically loaded components. Depending on the thermal expansion coefficient (α), glasses are divided into soft ($6 \cdot 10^{-6} – 12 \cdot 10^{-6}\ K^{-1}$) or hard ($< 6 \cdot 10^{-6}\ K^{-1}$) glasses. Soft glasses have low gas permeability but poor thermal shock resistance. With increasing SiO_2 content above 70 % and the addition of boron, glasses become harder. So-called borosilicate glasses have a low thermal expansion coefficient and high thermal shock resistance, which makes them a popular material in vacuum technology. For use at high temperatures (~1050 °C), quartz glass (pure SiO_2) is used. In general, technical glass can also be used for insulation purposes. In most cases, however, densely fired ceramics are used.

The selection of ceramics in vacuum technology is usually based on the operating temperature. While silicate ceramics are used up to 1350 °C, pure oxide ceramics are suitable up to 1800 °C. Aluminum oxide is most commonly used, for example in electrical feedthroughs or for insulation purposes within the vacuum system, and for complex geometries. The permeation depends mainly on the molecular diameters of the gas and the microstructure respectively the porosity of the ceramic. Permeation also increases with increasing temperature, which is the reason to coat ceramics with a glaze. This is done either with the enamel technique or a soft glaze on already finished components [5, 6].

2.2.3 Polymers

In general, the use of plastics in vacuum equipment should be avoided. The problems are mostly the water absorption, the low melting point as well as the high permeation. On the other hand, there is the electrical insulation and the easy machining aspect compared to other insulating materials such as ceramics or glass. For structural components, polyether ether ketone (PEEK) is a suitable material, for rough vacuum, polyoxymethylene (POM) may also be suitable. Polytetrafluorethylene (PTFE) or polyimides ("Kapton") can be used to insulate cables at medium temperatures, 280 °C and 250 °C respectively [14].

TU WIEN Bibliothek Your knowledge hub
Die approbierte gedruckte Originalversion dieser Diplomarbeit ist an der TU Wien Bibliothek verfügbar
The approved original version of this thesis is available in print at TU Wien Bibliothek.

Elastomers are most often used as sealants, in the simplest form as O-rings. Their deformability and recovery allow them to be re-used. Fluoroelastomers, designated FKM or FPM, and their derivatives such as FFKM are most suitable because of their low permeability and can be applied for systems up to a base pressure of about 10^{-8} mbar. A number of aspects must be considered when selecting suitable sealing materials: minimum and maximum temperature, permeability, outgassing and also chemical and UV resistance. Permeability is also highly dependent on temperature and the gas-species. Many graphs of permeability plotted over temperature can be found in the literature [5, 6, 14, 16, 17].

TU WIEN Bibliothek Your knowledge hub
Die approbierte gedruckte Originalversion dieser Diplomarbeit ist an der TU Wien Bibliothek verfügbar
The approved original version of this thesis is available in print at TU Wien Bibliothek.

2.3 Vacuum Pumps

Since the invention of the first vacuum pump by Otto von Guericke around 1650, many different types have been developed. The first experiments were done with a water pump, as a result, the term pump has prevailed for vacuum generation machines. However, gas compressor would be more accurate [5]. Application dependent, different types and combinations are used to remove gas particles out of sealed chambers. Vacuum Pumps are categorized due to their physical working principle in two types: gas transfer and gas capture pumps. The former works constantly, the latter needs to be regenerated due to the limited gas adsorption. Positive displacement pumps trap the gas in a volume and eject it at higher pressure after compression. Kinetic pumps accelerate gas particles towards the outlet, either by fast moving rotors or by fluid propellants. Figure 2.3 gives an overview of common used vacuum pumps.

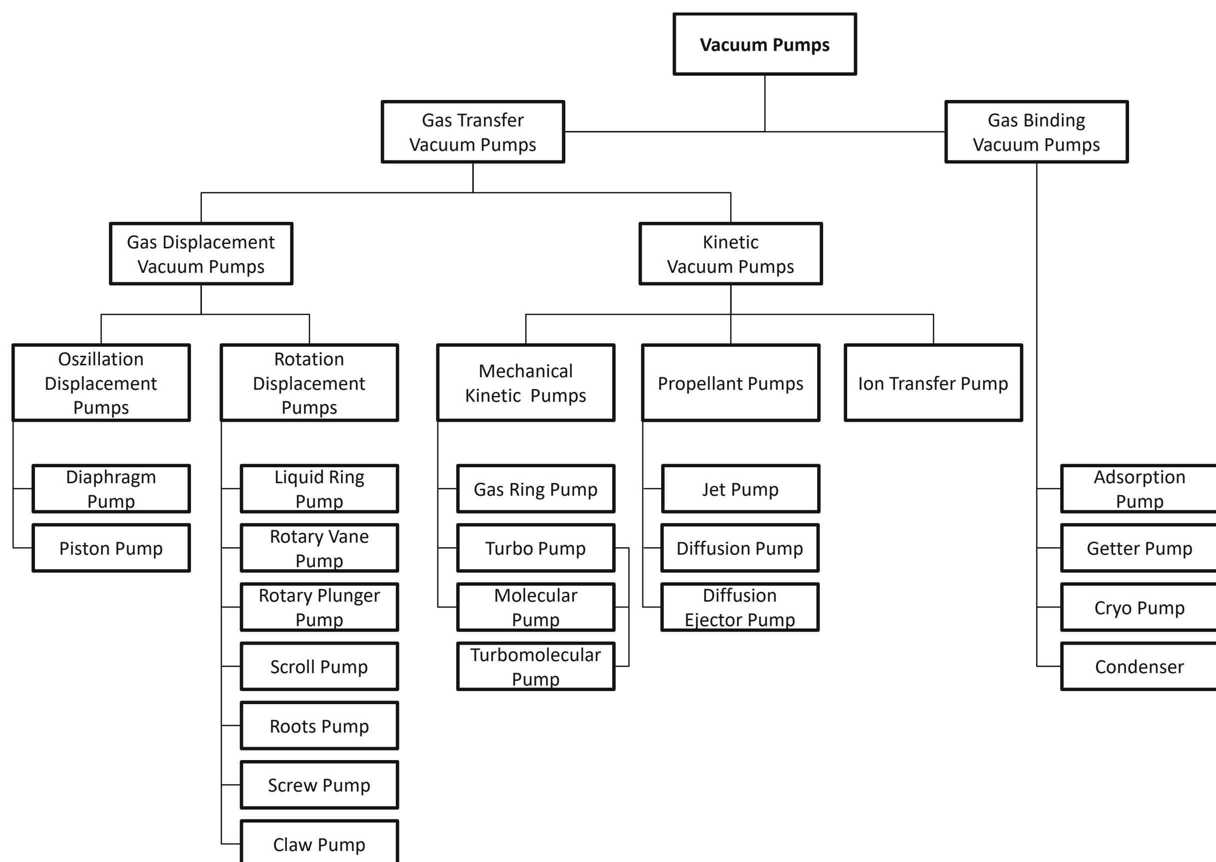

Fig. 2.3: Classification of vacuum pumps, adapted from [18,19].

Die approbierte gedruckte Originalversion dieser Diplomarbeit ist an der TU Wien Bibliothek verfügbar
The approved original version of this thesis is available in print at TU Wien Bibliothek.
TU WIEN Bibliothek Your knowledge hub

An overview of the working ranges of the different pumping principles is given in Figure 2.4. It is shown that at least two pumps must be combined to reach HV or UHV regions. Especially remarkable is the large working range of the turbomolecular pumps. This makes them suitable for a large number of applications and processes in a great variety of industries. The pumps used for PVD processes are briefly described below. Before that, some of the important characteristics of vacuum pumps will be explained. The determination of performance data of vacuum pumps is regulated in DIN ISO 21360-1 [20].

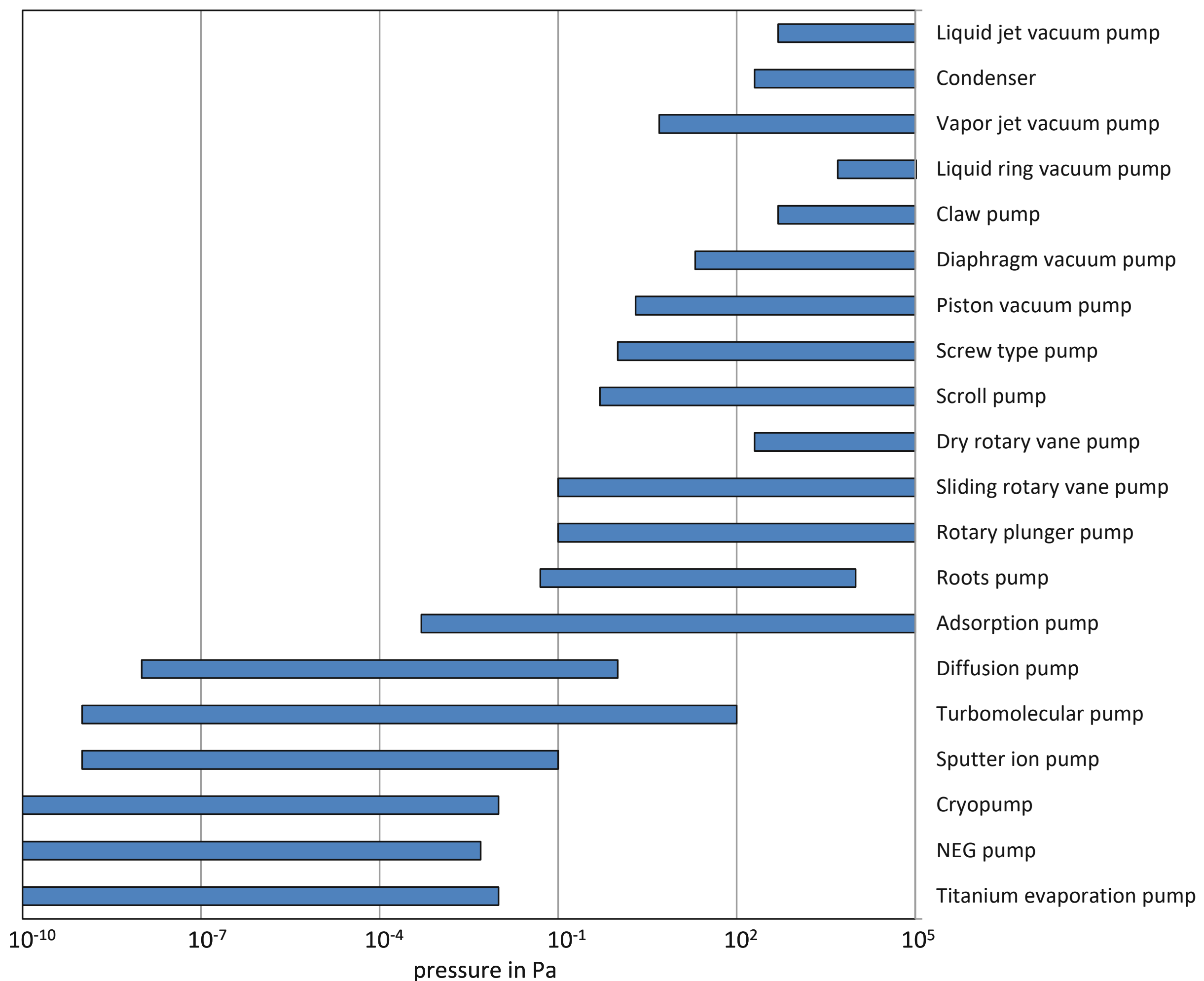

Fig. 2.4: Common working ranges of vacuum pumps, adapted from [5,19].

The pumping speed (S) represents the average volume flow through the suction port. It is dependent on the inlet pressure and is therefore shown in suction capacity diagrams above the suction pressure for suitable selection.

Die approbierte gedruckte Originalversion dieser Diplomarbeit ist an der TU Wien Bibliothek verfügbar
The approved original version of this thesis is available in print at TU Wien Bibliothek.
TU WIEN Bibliothek Your knowledge hub

$$S = \frac{dV}{dt} \tag{2.16}$$

The throughput (q_{pV}) is defined as the $p \cdot V$ flowrate of a gas as a function of the inlet pressure:

$$q_{pV} = \frac{dV}{dt} \cdot p \tag{2.17}$$

The ratio outlet to inlet pressure is the compression ratio (K). When determining, the suction flange is blind flanged and is designated K_0:

$$K_0 = \frac{p_o}{p_i} \tag{2.18}$$

Depending on the pumping principle and the necessary tolerances of moving components, there are losses due to the backflow of gas. The backflow conductivity (C_R) is calculated as follows:

$$C_R = \frac{S_0}{K_0} \tag{2.19}$$

For a two-stage pumping system, the following Equation (2.20) can be applied to calculate the total pumping speed, with S_V of the last stage and K_0 and S_0 of the previous stage [5, 21].

$$S = \frac{S_0}{1 - \frac{1}{K_0} + \frac{S_0}{K_0\, S_v}} \tag{2.20}$$

In the following sections the most important pump principles used for PVD systems are described. To achieve base pressures of 10^{-8} mbar, combinations of positive displacement pumps and turbomolecular pumps are used.

2.3.1 Rotary vane pumps

Rotary vane pumps are rotary displacement pumps. They operate against atmospheric pressure and can therefore be used as backing pumps. Single-stage pumps create vacuum of about 10^{-1} mbar, while two-stage pumps reach up to 10^{-3} mbar. In Figure 2.8 the working principle is shown schematically. The gas enters the working chamber (5) through the intake port (1). The eccentrically mounted rotor (3) contains two or more vanes (4) which are pressed against the housing wall (2) by centrifugal and resilient force, thus closing the working chamber. The divided working chamber is first enlarged until the second vane has passed over the inlet opening. Then the working area is reduced and the gas is compressed.

Die approbierte gedruckte Originalversion dieser Diplomarbeit ist an der TU Wien Bibliothek verfügbar
The approved original version of this thesis is available in print at TU Wien Bibliothek.
TU WIEN Bibliothek Your knowledge hub

The outlet valve (6) opens and the gas flows out, respectively into the second stage. In order to avoid or minimize backflow of gas, rotary vane pumps are driven with oil as working fluid. It must be ensured that there is no backflow of oil mist into the vacuum system. For this purpose, valves are also installed at the inlet, which then function as safety valves, but always remain open during operation.

If vapors such as water vapor are pumped, condensation may occur. This leads to a mixture with the working medium and increases the possible ultimate pressure. In addition, the vapors lead to corrosion. Therefore, it is important to operate pumps at higher temperatures according to the vapor-pressure curves of the pumped media. For example, if the gas ballast valve is open, the pump can be started before the chamber is evacuated to warm up. The operating medium can also absorb dust, but this further reduces the changing intervals, as is the case with condensate. It is important to select the appropriate oil, as this can be chemically decomposed. Where this, or the condensation of vapors, cannot be avoided, another pump type must be selected. A wide range of accessories can be used on and around rotary vane pumps: oil mist separators and oil feed backs, gas ballast valves, dust filters, activated carbon filters, catalyst traps or special chemical oil filters [21]. In order to avoid condensation of water vapor, and thus contamination of the operating fluid, in the low-pressure stage of rotary vane pumps, diaphragm pumps can be used as backing pumps. The diaphragm pump ensures backing pressure below the vapor pressure at corresponding operating temperatures. Therefore, the water condenses in the diaphragm pump, which is more suitable for this operation [22].

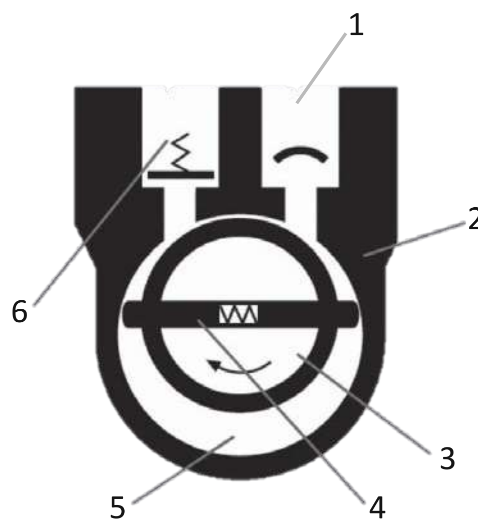

Fig. 2.5: Working principle of rotary vane pumps, adapted from [21].

Die approbierte gedruckte Originalversion dieser Diplomarbeit ist an der TU Wien Bibliothek verfügbar
The approved original version of this thesis is available in print at TU Wien Bibliothek.
TU WIEN Bibliothek Your knowledge hub

2.3.2 Diaphragm pumps

The further development of materials for diaphragm pumps in recent decades has made them suitable for use in high-purity applications. The diaphragms separate the working chamber from the drive chamber. Therefore, these dry positive displacement pumps are also suitable for use with a wide range of aggressive media, if appropriate materials are selected. Figure 2.6 shows the mechanical working principle. The diaphragm (1) is driven in an oscillating motion via a connecting rod (4) and the crankshaft. This changes the volume of the suction chamber (5). The inlet and outlet valves (6) open and close pressure-controlled. Dead space cannot be avoided, which leads to a poor compression ratio, as the residual gas remains in the suction chamber and reduces the intake volume. Models with several stages, serial or parallel coupled, can reach pressures below 1 mbar. In principle, diaphragm pumps are cost-effective for small, clean applications, e.g. in laboratories, with low necessary pump capacities [5, 21].

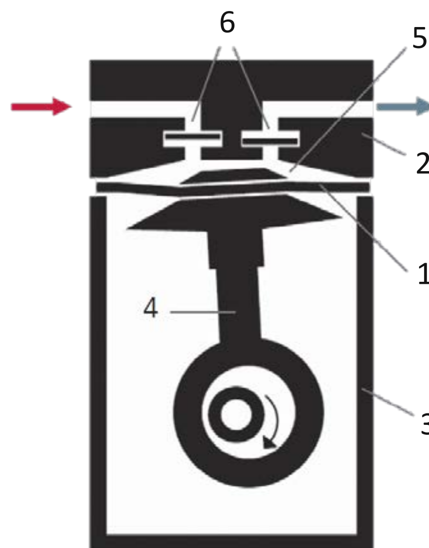

Fig. 2.6: Working principle of diaphragm pumps, adapted from [21].

2.3.3 Screw pumps

Screw pumps are the first twin-spool rotating positive displacement pumps mentioned here. The dry-running pump has two contactless screws (3) rotating in opposite directions (see Figure 2.7). The work volume is formed by the screw geometry. When using symmetrical screws, a controllable outlet side is required to raise pressure. Modern pumps use asymmetric screws where the thread pitch decreases towards the outlet. Thus, the gas is conveyed and

Die approbierte gedruckte Originalversion dieser Diplomarbeit ist an der TU Wien Bibliothek verfügbar
The approved original version of this thesis is available in print at TU Wien Bibliothek.
TU WIEN Bibliothek Your knowledge hub

compressed from the inlet (1) to the outlet (4). At the outlet, when used in rough vacuum, air flows into the displacement volume and is discharged again as the pump continues to rotate. The dissipated energy heats the pump and cooling is essential. Heating of the rotors is a problem compared to the cooled housing. Gaps between the rotors and the housing must be designed accordingly, but lead to a backflow of gas. With precise design and manufacturing, the gaps become very small at constant operating conditions. With large gas loads or high pressure, some heat is removed with the gas flow. For additional cooling, a gas ballast can be used, cooled gas can be recirculated, or rotors can be cooled directly from inside, for example with oil [5, 21].

Screw pumps can be used in a wide range. They are built with pumping speeds of 70 to 2500 m^3/h and work from ambient to 10^{-3} mbar. There is no contamination of working fluid in the vacuum vessel and these pumps are tolerant to dust and liquids. The efficiency is also good, which means that they are increasingly replacing rotary vane pumps in the higher pumping speed range.

Further optimizing the compression ratio has only limited advantages. Theoretically, one could choose a very large pitch gradient, but this would result in high power consumption, especially at high intake pressures. Even if the power consumption drops at lower intake pressures, disproportionally large engines would have to be installed [5].

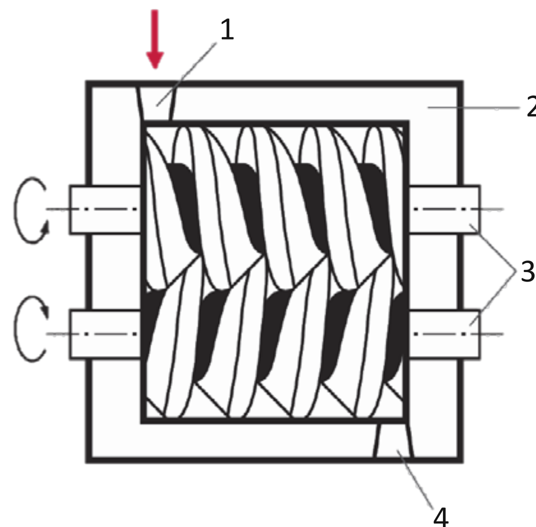

Fig. 2.7: Working principle of screw pumps, adapted from [21].

Die approbierte gedruckte Originalversion dieser Diplomarbeit ist an der TU Wien Bibliothek verfügbar
The approved original version of this thesis is available in print at TU Wien Bibliothek.
TU WIEN Bibliothek Your knowledge hub

2.3.4 Roots pumps

This type of pump became known as roots blower at the beginning of the 20th century. Two rotary lobe pistons with an eight-shaped profile rotate in opposite directions and convey the gas in the working chamber (3) to the outlet (2) (see Figure 2.8a). The coupling via a pair of gear wheels ensures the uniform contact-free movement of the rotors towards each other and towards the housing wall. The clearances are kept as small as possible and are adapted to the operating conditions of the dry-running system. Even with small designs, roots pumps achieve high pumping speeds through high rotational frequencies. However, the compression ratio is low and decreases further with increasing outlet pressure, as the backflow increases significantly. In addition, gas is delivered back to the suction side by adsorption and desorption. This effect becomes relevant at low back pressures. The compression ratio is highest in the range of 1 to 10 mbar outlet pressure due to these two opposite effects (see Figure 2.8b). Typically, backing pumps are used, which provide the main increase in pressure. Roots pumps can be designed as multistage pumps to handle larger pressure differences. This makes it even more important to avoid condensation of vapors and thus corrosion. For this purpose, pumps can be warmed up and possibly also operated with gas ballast.

Similar to screw pumps it is necessary to lubricate the bearings and the gear pair. Piston rings, labyrinth seals and radial shaft seals are used to prevent oil from entering the vacuum system. High pressure differences between the pump chamber and the oil reservoir can lead to leakage. This can be avoided by connecting the oil chamber to the suction side or the fore-vacuum side. Hermetic sealing to the outside is possible with magnetic couplings [5, 9, 21].

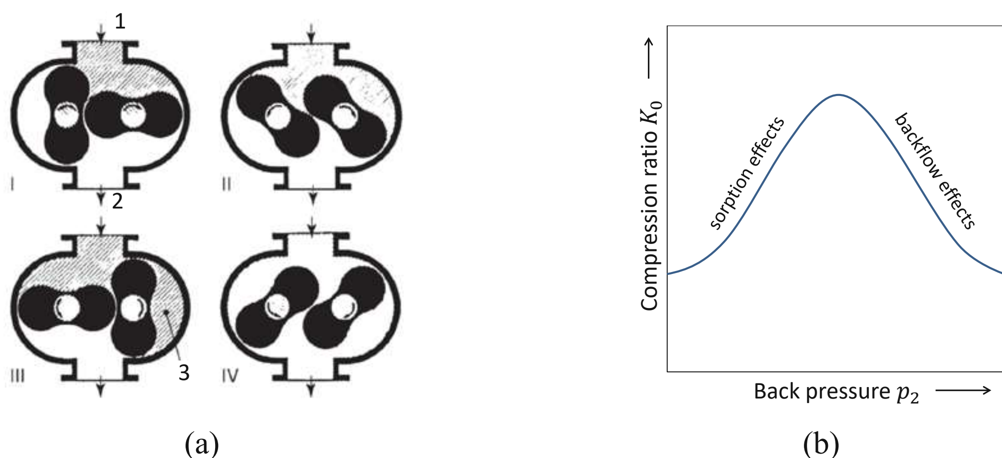

Fig. 2.8: (a) Working principle and (b) compression ratio of roots pumps, adapted from [5].

Die approbierte gedruckte Originalversion dieser Diplomarbeit ist an der TU Wien Bibliothek verfügbar
The approved original version of this thesis is available in print at TU Wien Bibliothek.
TU WIEN Bibliothek Your knowledge hub

2.3.5 Claw pumps

These pumps work similar to Roots pumps with two counter-rotating rotors. With the special geometry however, an internal compression is achieved, which makes the essential difference. Therefore, no outlet valves are needed. They run dry and contactless, synchronized via gears. The first claw pumps from Northey were built with one claw per rotor. This results in a dead volume of about 7 % and thus a poorer efficiency – with face side inlet and outlet. Further developments with asymmetrical rotors were able to overcome these volume losses. Nevertheless, profiles comparable to the Northey-type are still under investigation and optimization [23, 24]. Nowadays mainly exact profiles with two teeth per rotor are used. Figure 2.9 shows the working principle of a common claw pump with exact profiles, a main rotor (1) and a control rotor (2), the latter opens and closes the outlet. Flow losses can be further reduced by a radial inlet (6). The pump chamber is divided into four sections: the suction volume (3), two transport volumes (4) and the compression volume (5). From position I to IV the pressure remains constant, in V and VI the extracted gas is compressed and in VII and VIII almost completely ejected. Compared to the Northey-type, the remaining gas volume and dead volume is small. Consequently, the shown exact profile is more sensitive to condensation and dust loads. With single-stage pumps ultimate pressure of about 30 mbar is usually achieved. Models with up to seven stages are available. By adjusting the size ratio of the stages, the pumping speed characteristics and power consumption can be adapted to the process. Furthermore, claw pumps, as well as roots pumps, can be operated with speed control via frequency converter. This allows different pumping speeds to be covered for changing process conditions. Lower limits are set by backflow and required motor cooling; the upper limit is set by the thermal load of the pump [5].

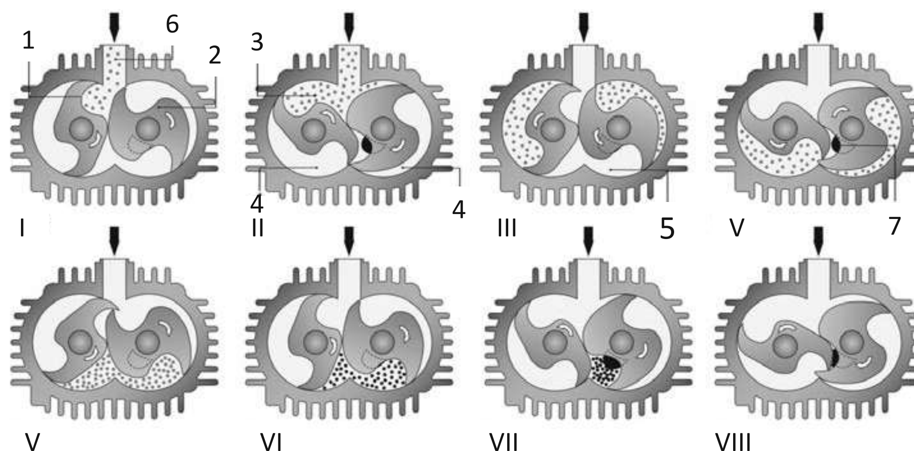

Fig. 2.9: Working principle of claw pumps, adapted from [18].

Die approbierte gedruckte Originalversion dieser Diplomarbeit ist an der TU Wien Bibliothek verfügbar
The approved original version of this thesis is available in print at TU Wien Bibliothek.
TU Bibliothek WIEN Your knowledge hub

Die approbierte gedruckte Originalversion dieser Diplomarbeit ist an der TU Wien Bibliothek verfügbar
The approved original version of this thesis is available in print at TU Wien Bibliothek.
TU WIEN Bibliothek Your knowledge hub

2.3.6 Turbomolecular pumps

Turbomolecular pumps are very popular for the generation of HV and UHV. Base pressures of 10^{-10} mbar can be achieved using suitable backing pumps. The transport of gas is based on the transmission of impulse and the associated movement of the gas particles towards the outlet. The operating principles of turbopumps are described in DIN 28400-2 [19]. The working principle is coupled to the laws of molecular flow, large λ are required for directed transport. Therefore, these pumps cannot operate against atmospheric pressure and backing pumps are required. Turbomolecular pumps consist of several fast-rotating rotor blades and inversely mirrored stator blades. Additionally, turbomolecular pumps are often equipped with molecular pumping stages according to the Gaede principle (Gaede, Holweck or Siegbahn stages), referred to as compound pumps. This enabled ejection at higher pressure and the use of cheaper backing pumps. The Gaede principle follows the theory that gas particles are adsorbed for a short dwell time when they hit a wall before they are desorbed again. As this wall moves, the speed component is superimposed by the circumferential speed. The movement thus directed means gas flow and pumping effect [5].

The compression ratio of turbomolecular pumps can be estimated using the Equation (2.21), considering Figure 2.10. The factor g ($1 < g < 3$) describes the free path until the next collision with the wall, u is the circumferential speed of the blades and $\bar{c}$ is the thermal velocity according Equation (2.10). K_0 increases exponentially with u and $\sqrt{M}$, therefore heavier gases, e.g. nitrogen, are pumped easier than hydrogen [5, 21].

$$K_0 = \exp\left(\frac{1}{g} \cdot \frac{1}{\sin\alpha} \cdot \frac{u}{\bar{c}}\right) \tag{2.21}$$

The pumping speed S_0 depends on the suction surface (A), the average circumferential speed (u) and the blade angle (α).

$$S_0 = \frac{1}{4} A\, u \sin(2\alpha) \tag{2.22}$$

The effective pumping speed (S_{eff}) is reduced by the conductance of the inlet flange. Assuming an ideal α of 45° for heavy gases (M > 20 g/mol) S_{eff} is approximately:

$$S_{eff} = \frac{A\ u}{4 \cdot (\frac{u}{\bar{c}} + 1)} \tag{2.23}$$

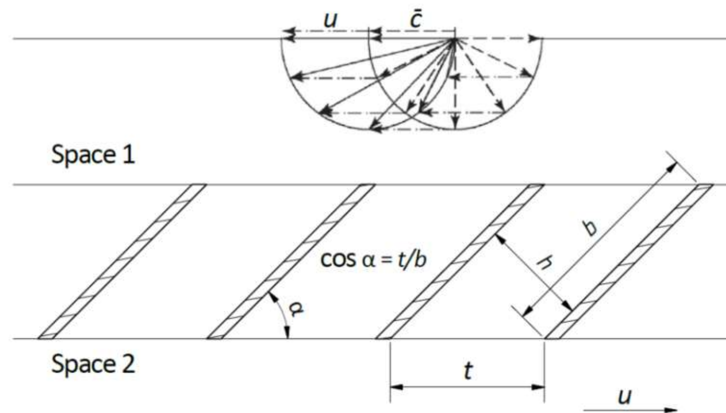

Fig. 2.10: Blade geometry of turbomolecular pumps, adapted from [5].

High rotation speeds (up to 90.000 rpm) lead to high mechanical stresses. Therefore, rotors must be made of highly loadable materials. Due to the low density and relatively high strength, usually aluminum alloys are used. Here, the thermal load must be taken into account to prevent creep. Thermal input occurs mainly through gas friction. Especially with heavy noble gases, temperature rises in the blades by up to 200 °C. Bearings are another challenge. Smooth, precise running is required to maximize the effectiveness of turbopumps with tight tolerances and minimal gaps. Magnetic bearings or combinations with ceramic bearings are used for this purpose. Oil-lubricated ball bearings can be used in the low-pressure zone but are not that common anymore [5].

Die approbierte gedruckte Originalversion dieser Diplomarbeit ist an der TU Wien Bibliothek verfügbar
The approved original version of this thesis is available in print at TU Wien Bibliothek.
TU WIEN Bibliothek Your knowledge hub

2.4 Vacuum Pressure Analysis

In vacuum technology, pressure gauges must cover a wide range of over 15 decades – from 1000 mbar to 10^{-12} mbar providing necessary insides to the predominant conditionals. Individual measuring systems only cover certain regions, making it necessary to combine different measuring cells, see Figure 2.11. A distinction is made between direct and indirect systems. In direct measuring systems, elastic deformation, for example of a membrane, is detected. Indirect systems measure pressure-dependent properties such as thermal conductivity, viscosity or ionized particle density (also via voltage-current analysis). Therefore, these instruments are always dependent on the type of gas and have a limited suitability for monitoring processes. The most important measuring methods used in PVD based deposition systems are described below [9].

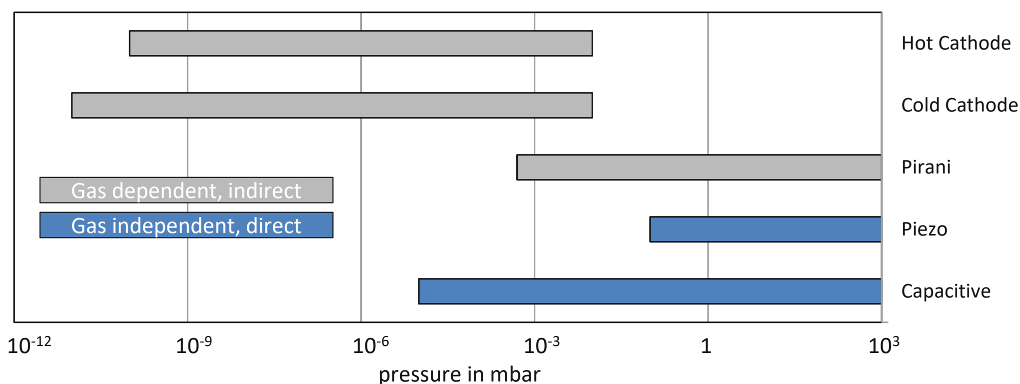

Fig. 2.11: Theoretical working ranges of direct and indirect measurement principles.

2.4.1 Capacitive diaphragm vacuum manometers

Capacitive membrane vacuum gauges use the membrane directly as part of a plate capacitor. The direct pressure depending distance between the membrane and the fixed electrode causes a measurable change in capacitance (see Figure 2.12a). The diaphragm can be made of ceramic (mainly Al_2O_3) with a thin metal layer, stainless steel or Inconel. Diaphragms of different thickness can cover different ranges; the lower limit is at 10^{-5} mbar, because of high temperature influences and the low forces. The temperature errors can either be compensated electrically or the transmitter can be kept at a constant temperature by heating [9].

Die approbierte gedruckte Originalversion dieser Diplomarbeit ist an der TU Wien Bibliothek verfügbar
The approved original version of this thesis is available in print at TU Wien Bibliothek.
TU WIEN Bibliothek Your knowledge hub

2.4.2 Piezo vacuum gauges

Piezo resistive diaphragm vacuum gauges use the principle of strain gauges to determine the deflection of the pressure-loaded diaphragm. The strain gauge is stretched with the membrane, subsequent its electrical resistance changes and is measured (see Figure 2.12b). To increase the sensitivity, several strain gauges are connected in a Wheatstone bridge arrangement. The amplifier electronics is directly integrated in the transducer head and converts the signal into a standardized measuring signal, as with other measuring systems. These are mostly analog signals of 4 - 20 mA according to DIN IEC 60381-1 [25], possibly also 0 - 10 V after DIN IEC 60381-2 [26]. Piezo pressure transducers can be used for absolute and gauge pressure. They are robust and insensitive to rapid pressure changes and have a good accuracy. However, the temperature drift must be taken into account [9].

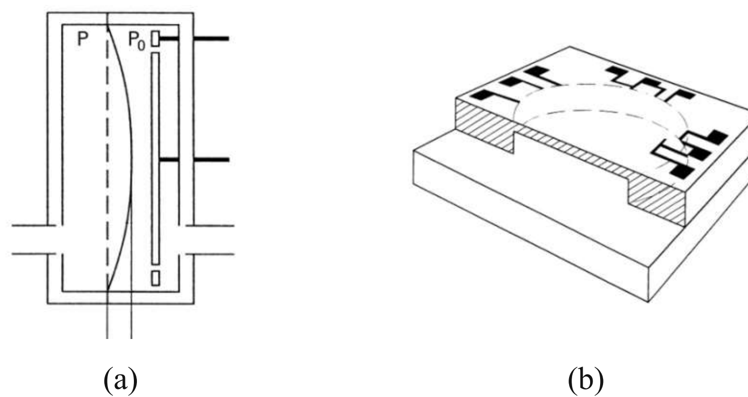

Fig. 2.12: Working principle of (a) capacitive vacuum gauge and (b) piezo resistive vacuum gauge, from [21].

2.4.3 Pirani vacuum gauges

Pirani vacuum gauges are thermal transfer gauges. The thermal conductivity of gases depends on the particle number density and therefore also on the pressure. The distance between the surfaces must be much larger than the mean free path. A filament (usually made of tungsten) is electrically heated in a tube to a constant temperature. Heat is dissipated by conduction to the tube wall, the power to maintain the filament temperature is measured. The Pirani principle can be used in ranges from atmosphere to 10^{-4} mbar. From the lower limit up to 1 mbar, the gas species-dependent thermal conductivity can be corrected with a factor due to its almost linear behavior, see Figure 2.13. Usually these pressure transmitters are calibrated for nitrogen or air as these are the most common atmospheres [9].

Die approbierte gedruckte Originalversion dieser Diplomarbeit ist an der TU Wien Bibliothek verfügbar
The approved original version of this thesis is available in print at TU Wien Bibliothek.
TU WIEN Bibliothek Your knowledge hub

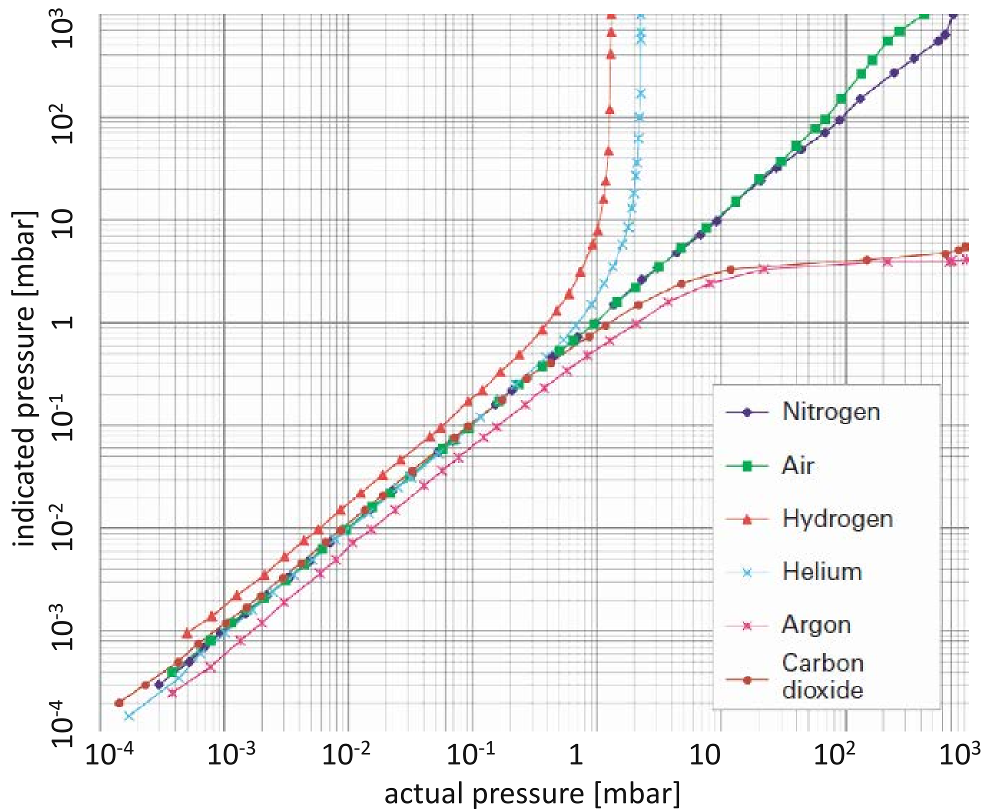

Fig. 2.13: Pirani vacuum gauge curves for calibration, taken from [21].

2.4.4 Cathode ionization vacuum gauges

Ionization vacuum gauges determine the pressure indirectly via the particle number density, more precisely via the number of ionized gas particles. In so-called cold cathodes, a high direct current (DC) voltage is applied between two electrodes. Electrons leave the cathode and ionize neutral gas particles on their way to the anode. A gas discharge is ignited and this current is analyzed subsequently. The principle of the inverted magnetron is used to ensure that enough particles are ionized even at a pressure below 1 mbar. The applied magnetic field causes the electrons to move on a spiral path, the distance to the anode increases and more collisions and ionization takes place. The probability of ionization depends on the type of gas, thus also the measured pressure level. Contamination of cold cathodes must be avoided. For this purpose, the gauge must not be operated at pressures above 0.1 mbar. A residual gas atmosphere containing hydrocarbons must be avoided, and argon loads lead to sputtering of the cathode. External magnetic field interference will also change the measurement result, or the magnetic field can disturb other equipment [5, 21].

Die approbierte gedruckte Originalversion dieser Diplomarbeit ist an der TU Wien Bibliothek verfügbar
The approved original version of this thesis is available in print at TU Wien Bibliothek.
TU WIEN Bibliothek Your knowledge hub

In hot cathode ionization vacuum gauges, the electrons are generated by a heated cathode. The best most widely used type is the Bayard-Alpert gauge. A voltage is applied between the heated cathode and the anode to accelerate the electrons towards the anode. The ions generated by collisions with the electrons impinge on a collector. The emission current and the collector current can be measured and the pressure can be determined. The gas type-dependent measuring accuracy of about ±10 % is much more accurate than that of cold cathodes with ±25 % [5, 21].

Die approbierte gedruckte Originalversion dieser Diplomarbeit ist an der TU Wien Bibliothek verfügbar
The approved original version of this thesis is available in print at TU Wien Bibliothek.
TU WIEN Bibliothek Your knowledge hub

3 Physical Vapor Deposition

Surface modification has been used since the middle of the last century to selectively improve properties of materials. A wide variety of applications have been optimized or even made possible in the first place. Thin films are deposited to produce hard surfaces, optical layers, electronic components or decorative elements, in other words to enhance the limited properties of bulk materials. Especially, mechanically stressed parts can thus be improved for increasingly challenging applications and thus also contribute to material savings and, through better efficiency and durability. Physical vapor deposition (PVD) is one of the most understood and widely used processes for depositing thin films [7]. The coating process involves three steps: formation of a vapor, transportation of these species and condensation and film growth. In this thesis only sputtering, a subarea of PVD technology is described in detail. An overview of all well-known processes used in thin film technology is shown in Figure 3.1.

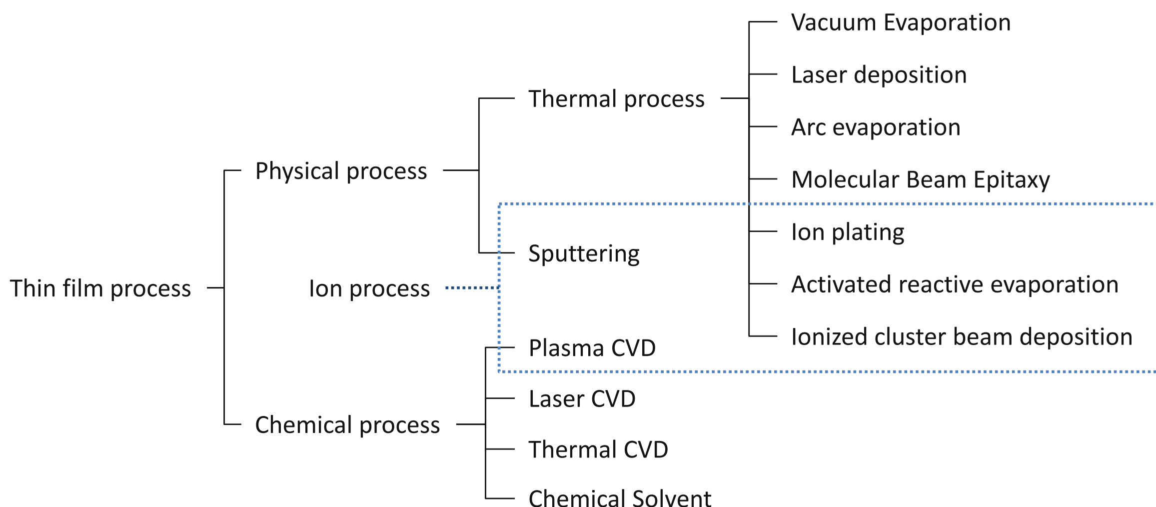

Fig. 3.1: Thin film deposition techniques, adapted from [7].

Die approbierte gedruckte Originalversion dieser Diplomarbeit ist an der TU Wien Bibliothek verfügbar
The approved original version of this thesis is available in print at TU Wien Bibliothek.
TU WIEN Bibliothek Your knowledge hub

3.1 Sputtering

The sputtering process is based on the physical ejection of surface atoms or molecules from a solid (or liquid) target material due to the transfer of momentum introduced by the bombardment of charged particles. The impinging species are typically gaseous ions – mainly inert gas ions – generated in a glow discharge, which are accelerated onto the target surface through the applied electric field. In general, plasmas are composed of ionized species, electrons and neutral atoms next to each other, whereas the overall charge is neutral. In a classic glow discharge set-up, the plasma is ignited by a high potential difference between the cathode and anode using inert (and heavy) gas atmospheres (so-called "working gas") at low pressures. Argon is widely used as working gas, due to cost and availability issues for other noble gases such as Krypton or Xenon [27]. By applying a high negative DC voltage to the cathode (and thus to the target), a negative glow discharge in the surface near region can be observed (see Figure 3.2a). Important for the sputter process is the cathode and negative glow. Ar is ionized by collision with electrons to Ar^+ and a chain reaction occurs as further electrons are released. Ar^+ is attracted and accelerated by the negative voltage towards the cathode and hence the target material. Next to the ejection of target atoms, also further processes are initiated, e.g. secondary electron emission. These now move towards the substrate and deposit a new thin film. There is also ion implantation and heating at the target, but this is not desirable. Important influencing factors are the angle of impact, the surface and binding energy of the target material, the pressure, the applied voltage and the distance to the substrate. The sputter yield (Y) is defined as the number of ejected atoms in relation to the impinging ions and is an indicator of the efficiency of the process. There are different approaches to calculate Y. The mass (M_I) and kinetic energy (E_I) of the ion and the mass of the sputtered target atom (M_T) influence Y as well as the binding energy of surface atoms (U_S) and the incidence angle. Y is hardly affected by the target temperature. A minimum threshold energy (E_{th}) is necessary for the sputtering process to work, see Figure 3.2b. When the mass of the ion equals the mass of the target, (E_{th}) becomes high. An estimation of Y in the region near the threshold is given in Equation (3.1). α is a dimensionless factor representing the mass ratio and ion energy [27–30].

$$Y = \frac{3}{4\,\pi^2}\,\alpha\,\frac{4\,M_I\,M_T}{(M_I + M_T)^2}\,\frac{E_I}{U_s} \tag{3.1}$$

Die approbierte gedruckte Originalversion dieser Diplomarbeit ist an der TU Wien Bibliothek verfügbar
The approved original version of this thesis is available in print at TU Wien Bibliothek.
TU WIEN Bibliothek Your knowledge hub

Due to ion implantation, the sputter yield cannot be increased infinitely and reaches maximum values in the range of ~10 keV ion energy. The energy of the sputtered atoms is in the range of several eV, but about 10 times higher than that of evaporated atoms, for example [27].

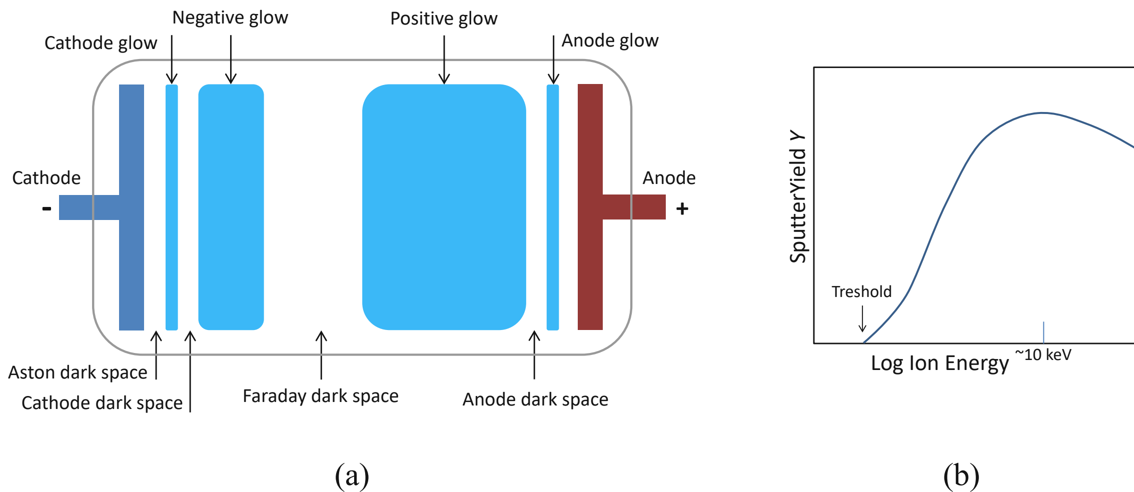

(a) (b)

Fig. 3.2: (a) structure of glow discharge in PVD sputter systems; (b) sputter yield; adapted from [28] and [27].

Only conductive targets can be used in DC sputtering, which is one main disadvantage and a strong limitation besides the very high required voltages. Nevertheless, DC sputtering achieves high deposition rates. Non-conductive materials or materials with a high resistance would require a high DC voltage to sustain a plasma – although thermal heating also limits these processes. For alternating current (AC), however, different physical laws apply. The impedance of dielectric capacitance decreases with increasing frequency. AC can therefore be conducted through non-conductive materials and a glow discharge can be maintained. The movement of electrons and ions is equal/contrary to the oscillating electric field. However, the electrons are more mobile than ions due to electromagnetic properties In RF driven process the surface area of the cathode compared to the anode play a crucial role, to sustain effective sputter processes [30].

Die approbierte gedruckte Originalversion dieser Diplomarbeit ist an der TU Wien Bibliothek verfügbar
The approved original version of this thesis is available in print at TU Wien Bibliothek.
TU WIEN Bibliothek Your knowledge hub

3.2 Reactive Magnetron Sputtering

Due to many advantages over conventional methods, magnetron sputtering is a widely used and the most common process. In conventional DC sputtering, quite high voltage and high pressures are needed to maintain a stable glow discharge, exhibiting the disadvantage of more collisions of the sputtered species on the way to the substrate – considering the mean free pathway (Equation (2.11)). As a result, the deposition rate is low due to scattering at a high energy input. By placing magnet systems behind the target (magnetic field lines hit the target surface perpendicular), more electrons are trapped near the target surface and the plasma is kept stable even at low voltages. More Ar is ionized at lower Ar pressure and the plasma density increases. The Lorentz force directs the electrons along a circular path, in the case of round targets. Y is higher in this area of the target and thus the so-called racetrack is formed.

The arrangement and strength of the magnet systems affect Y and also the ion bombardment on the substrate, which results in different film growth and thus possibly improved properties of deposited thin films. To support this effect, a negative voltage is applied to the substrate, the so-called bias potential. Balanced and unbalanced magnetrons are used and differ in the arrangement and strength of the outer and inner magnet, as shown in Figure 5.7. Ideally, the magnetic field lines close between the inner and outer magnet in a conventional balanced magnetron. The reflux of the field lines takes place through the steel yoke below the magnet system. In the case of the unbalanced magnetron, the magnetic field lines are partly directed away from the magnetron, and thus from the target, towards the substrate.

Magnetic fields can be generated by permanent magnets (e.g., AlNiCo or NdFeB) or electromagnets. The latter are limited in magnitude by self-heating. Permanent magnets do not necessarily require cooling, but they may only be operated below the Curie temperature, otherwise they may lose their magnetism permanently. In any case, cooling of the target is necessary, so the magnets can be kept at constant low temperatures.

A major disadvantage of conventional magnetron sputtering is the poor target utilization, due to the abovementioned race track formation. Different approaches are applied in order to achieve a more uniform surface removal: adjustable electromagnets, race track shaped targets or rotating cylindrical magnetrons with tubular targets – just to mention a few examples [27, 28, 30, 31].

Die approbierte gedruckte Originalversion dieser Diplomarbeit ist an der TU Wien Bibliothek verfügbar
The approved original version of this thesis is available in print at TU Wien Bibliothek.
TU WIEN Bibliothek Your knowledge hub

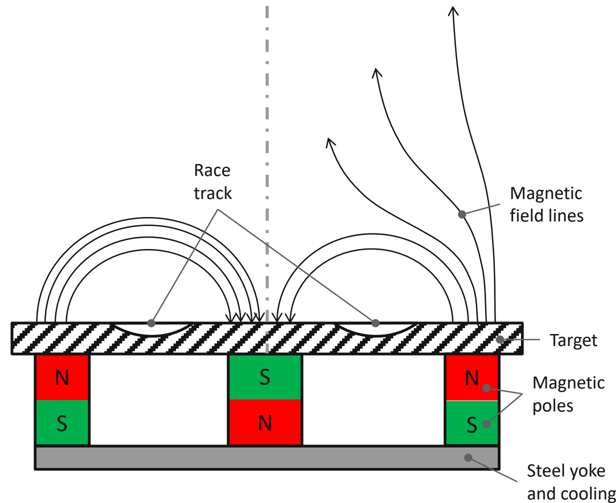

Fig. 3.3: Balanced (left) and unbalanced magnetron (right), adapted from [31].

The sputtering process allows a wide variety of thin film systems. Metallic, alloyed or compound targets can be used to synthesize layers on various substrates. However, this is associated with the difficulty of maintaining and adjusting the chemical composition on both the substrate or the deposited thin film, and the target surface. Surface diffusion is one driving process during film growth, effecting the chemical composition of the arriving species obtaining different atomic masses as well as sputter yields. Especially, ceramic targets obtain high work functions and non-ideal electrical properties, which also strongly effects the sputter yield. To partly avoid these problems, the introduction of reactive gas can help to grow non-metallic films. Therefore, so-called reactive sputtering is explained in the following. In most cases gases in a molecular state (e.g., N_2, O_2, C_2H_2, etc.) are introduced into the recipient at low partial pressure and react with the sputtered species to form compounds onto the substrate. Thus, electrically conductive targets can be used to produce non-conductive coatings such as TiN or TaC.

Simultaneously the presence of reactive gases leads to the so-called poisoning of the target because of the formation of compounds also on its surface. Poisoning results in lower Y, instable glow discharge or even break down and arcs. To overcome this problem different sputter configurations like pulsed DC voltage and monitoring of reactive gas with residual gas analyzers are used nowadays.

Die approbierte gedruckte Originalversion dieser Diplomarbeit ist an der TU Wien Bibliothek verfügbar
The approved original version of this thesis is available in print at TU Wien Bibliothek.
TU WIEN Bibliothek Your knowledge hub

3.3 Film Growth

The excellent properties of thin films are significantly related to film growth and thus to its influencing parameters during the process. The most important factors are the temperature, pressure, bias voltage and the material and surface properties of the substrate. The microstructure is described by the grain size, crystallographic structure, phase composition, lattice defects and surface morphology. The coating temperature is mostly far below the melting point, thus layer growth does not take place at thermodynamic equilibrium. In this way it is possible to produce metastable phases due to extremely high cooling rates in the range of 10^{13} K/s. Film growth starts with condensation on the surface and the subsequent surface diffusion and nucleation of the sputtered species. A distinction is made between three growth mechanisms: island growth, layer growth and a combination of both, which are depending on thermodynamics and kinetics [32].

Good ways to illustrate the layer growth of thin films based on the most important parameters are the so-called structure zone diagrams (SZD). These are applicable to a variety of polycrystalline thin films. Already in 1969 a model was presented by Movchan and Demchishin for relatively thick films made via evaporation processes [33]. The basis of this diagram, as for all further introduced ones, is the homologous temperature (T_h). The homologous temperature is defined as the temperature of the process in relation to the melting temperature (T_m) of the deposited material – see Equation 3.2.

$$T_h = T/T_m \tag{3.2}$$

The main statement of the SZD by Movchan and Demchishin is the classification into three areas based on T_h. In the first zone ($T_h < 0.3$) the mobility of the adatom is low, resulting in a fine-grained structure of the textured grains towards the incoming adatom species with rounded tips. At higher temperatures ($0.3 < T_h < 0.5$), surface diffusion increases, resulting in more uniform and larger columnar grains. In the third zone ($T_h > 0.5$) bulk diffusion and recrystallization sets in, resulting in dense films with large grains.

Barna and Adamik [34] have introduced a transition zone in the low temperature range ($T_h \sim 0.3$) and described the competitive growth texture zone, where surface diffusion occurs slightly at grain boundaries. Layers of this zone show excellent properties: small polycrystalline grains and a dense smooth surface. Thornton [35] has published a SZD that also includes the pressure. The differences can be described by the pressure-dependent kinetic energy of the impinging adatoms. Messier [36] has replaced the pressure by the ion energy in

Die approbierte gedruckte Originalversion dieser Diplomarbeit ist an der TU Wien Bibliothek verfügbar
The approved original version of this thesis is available in print at TU Wien Bibliothek.
TU WIEN Bibliothek Your knowledge hub

his SZD by adding the bias voltage. Nowadays, Anders' SZD [37] is the preferred choice because it describes the ion-assisted film growth also considering the removal via etching (see Figure 3.4). The axes have been generalized as follows: T_h is replaced by the generalized temperature T^*. This now includes T_h and the temperature shift due to the potential energy of the incoming particles on the surface. The p axis is replaced by a logarithmic axis E^*, the normalized energy, which describes the displacement and heating effects due to the kinetic energy of the incoming particles. The third axis t^* shows the layer thickness and the possible "negative layer thickness", i.e. ion etching [7, 37, 38].

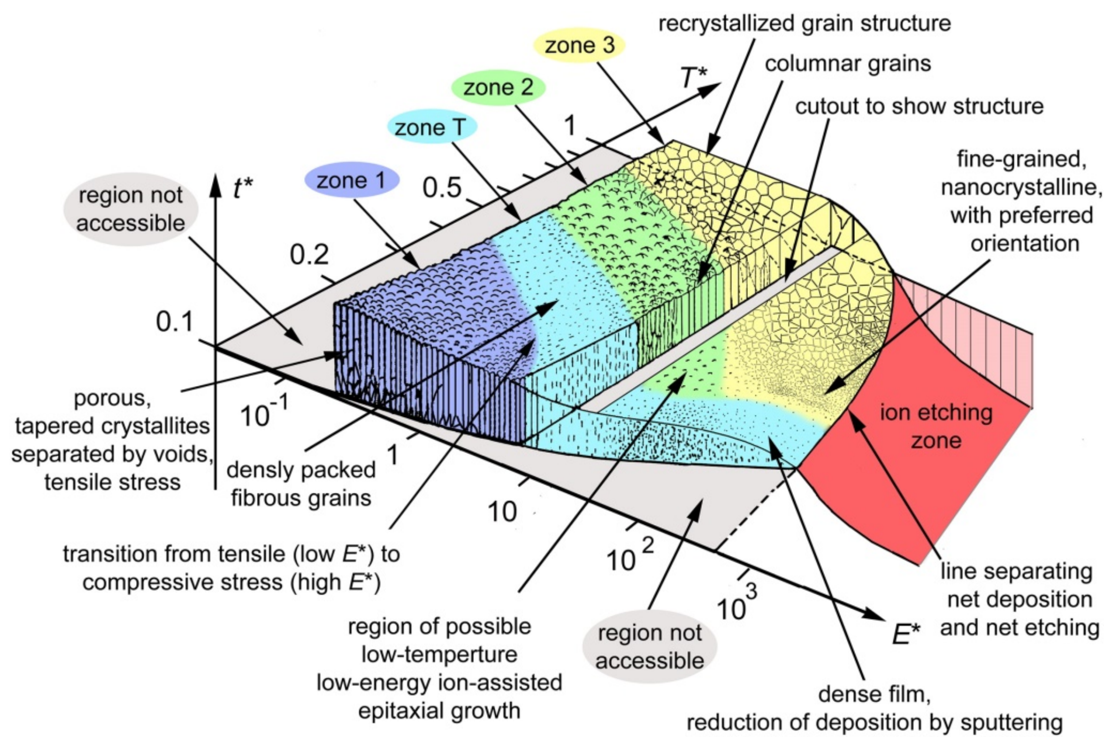

Fig. 3.4: Structure zone diagram by A. Anders [37].

Die approbierte gedruckte Originalversion dieser Diplomarbeit ist an der TU Wien Bibliothek verfügbar
The approved original version of this thesis is available in print at TU Wien Bibliothek.
TU WIEN Bibliothek Your knowledge hub

4 Diamond-Like Carbon

Since the first publications on amorphous carbon films in the mid-1950s, diamond-like carbon (DLC) films have established themselves as the best solutions in a variety of applications. Due to the extremely high compressive stress state of DLC layers independent on the substrate material, these coatings were only used after intensive research and further development on adhesion layers (mainly Cr, Ti, Ta, and Si) around the 1990s. DLC coatings combine high hardness and wear resistance at low coefficient of friction, chemical inertness and optical transparency in the infrared spectral range. Therefore, they are used in diverse industrial applications, especially in the automotive sector, to improve tools and components and make them more durable. DLC is also used as protective coating for cutting and forming tools, for biomedical components or as dielectric layers [1, 28, 39].

Generally, DLC coatings are produced by PVD or chemical vapor deposition (CVD) techniques. Based on the synthesis method, different types of materials with varying bonding characteristics and hence properties can be distinguished. A classification of DLC coatings to standardize the designations is made in the VDI guideline 2840 [40]. The distinguishing characteristics are as follows: amorphous or crystalline layers, the hydrogen content, the predominant part of the C-C bond (sp^2 or sp^3 hybridized) and the modification with additional metals or non-metals. The most important PVD-DLC layers with their abbreviations, designations and main bonding characteristics are listed below [40]:

- a-C: hydrogen free amorphous carbon film; sp^2; “graphite like carbon”
- ta-C: tetrahedral hydrogen free amorphous carbon film; sp^3; “amorphous diamond”
- a-C:Me: metal containing hydrogen free amorphous carbon film; sp^2; “metal-DLC”
- a-C:H: hydrogenated amorphous carbon film; sp^2 or sp^3; “hard carbon”
- ta-C:H: tetrahedral hydrogenated amorphous carbon film; sp^3; “DLC”
- a-C:H:Me: metal containing hydrogenated amorphous carbon film; sp^2; “metal DLC”
- a-C:H:X: modified hydrogenated amorphous carbon film; sp^2; “DLC”

Die approbierte gedruckte Originalversion dieser Diplomarbeit ist an der TU Wien Bibliothek verfügbar
The approved original version of this thesis is available in print at TU Wien Bibliothek.
TU WIEN Bibliothek Your knowledge hub

The metal components (Me) are typically W, Cr or Ti, the modifying components (X) can be Si, O, N, F or B. Bewilogua [1] has tabulated a comparison of the most important layers with diamond and graphite, see Table 4.1.

Table 4.1: Typical properties of diamond, DLC coatings and graphite, from [1].

Crystal system	**Diamond**	**ta-C**	**a-C:H**	**Graphite**
	Diamond cubic	Amorphous	Amorphous	Hexagonal
Mass density [g/cm³]	3.51	2.5 - 3.3	1.5 - 2.4	2.26
sp³ content [%]	100	50-90	20 - 60	0
Hydrogen content [at.%]	0	~1	10 - 50	0
Hardness [GPa]	100	50-80	10 - 45	<5
COF in humid air	0.1	0.05 - 0.25	0.02 - 0.3	0.1 - 0.2
COF in dry air	0.1	0.6	0.02 - 0.2	>0.6
Band gap [eV]	5.5	1 - 2.5	1 - 4	-0.04
El. resistivity [Ωcm]	10^{18}	10^{6} - 10^{10}	10^{4} - 10^{12}	10^{-6} - 10^{-2}
Thermal stability in air [°C]	800	400 - 600	300 - 350	>500

DLC coatings with high hardness should contain a high percentage of sp³ bonded C – in relation to perfect diamond being fully sp³ hybridized – and a low amount of H, leading to a more amorphous morphology. In contrast, coatings with a low COF might have a high content of H and sp² bonded C. Highest amounts of sp³ hybridized C in ta-C (~ 88 %) can be achieved by plasma-enhanced CVD (PECVD) processes [41]. A useful method to depict the different compositions of DLC layers is the ternary phase diagram shown in Figure 4.1.

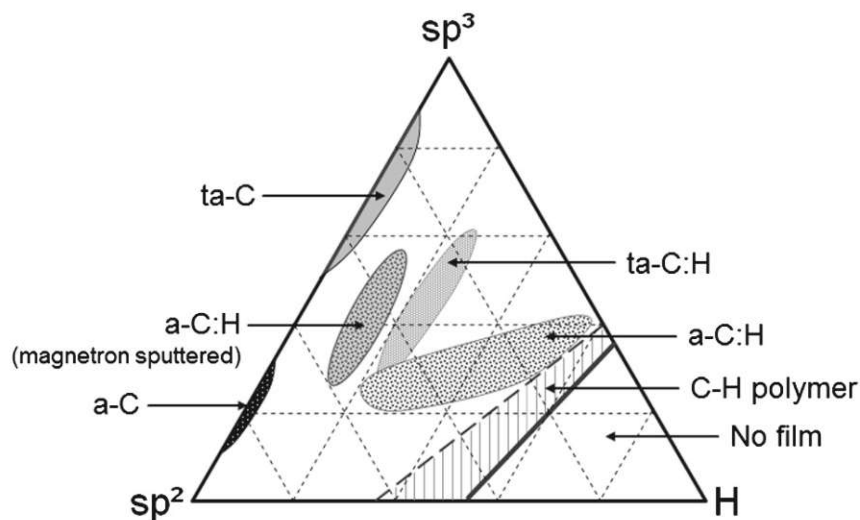

Fig. 4.1: Ternary phase diagram of DLC films assuming sp² and sp³ hybridized carbon and H to form DLC coatings, from [1].

Die approbierte gedruckte Originalversion dieser Diplomarbeit ist an der TU Wien Bibliothek verfügbar
The approved original version of this thesis is available in print at TU Wien Bibliothek.
TU WIEN Bibliothek Your knowledge hub

A. Erdemir [42] proofed the positive effect of high hydrogen contents on the tribological properties of DLC coatings. Different gases (e.g., C_2H_2) or gas mixtures (e.g., $CH_4 + H_2$) were introduced in plasma assisted CVD (PACVD) processes to compare the obtained coatings in tribological tests. Coatings made from gas with a high H/C ratio of about 10 achieved COF < 0.005 in an inert atmosphere, which is 200-times less compared to H-free layers. However, the COF changes negatively for high H containing DLC layers under normal environmental conditions (moist air). Conversely, however, friction improves for H-free coatings under ambient conditions, see Figure 4.2.

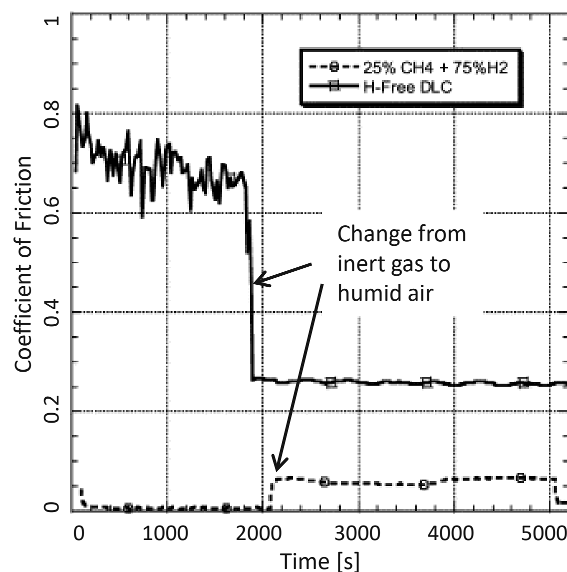

Fig. 4.2: Effect of humidity on COF: H-free and hydrogenated DLC films, adapted from [42].

Different approaches are followed to adjust mechanical and tribological properties with the ratio of sp^3/sp^2 hybridized DLC layers. Nakamura et al. [43, 44] have investigated the change in composition by varying the substrate bias voltage. It has been shown that the number of sp^3 bonds decrease with increasing bias voltage (0 to -300 V) in unbalanced magnetron sputtered films. Nevertheless, the indentation modulus and hardness increase with increasing bias voltage, with maximum values at -200 V. This relation is explained by the changed layered structure due to the ion bombardment during layer growth. However, this has a negative effect on the coating adhesion, as the compressive stresses in the thin film increase. To improve the adhesion of DLC films, metallic bonding layers such as Cr, Ti, Ta or W are deposited. These metals are beneficial as they tend to form stable carbides [41, 45–49]. CrN interlayers are also well established, or the doping of DLC layers like a:C:H:Me prepared by reactive magnetron sputtering [46, 47, 50].

Die approbierte gedruckte Originalversion dieser Diplomarbeit ist an der TU Wien Bibliothek verfügbar
The approved original version of this thesis is available in print at TU Wien Bibliothek.
TU Bibliothek WIEN Your knowledge hub

5 Design of the PVD System ”Frida”

The magnetron sputter system "Frida" was developed as a research facility for coating development within the Thin Films Materials Science Division of the TU Wien. In particular, the request for a recipient for reactive sputtering of carbon films was addressed. The requirements for the system are listed below.

Vacuum system:

- Small, cheap chamber, preferred spherical from stock.
- UHV design, base pressure below 10^{-6} mbar.
- One coating per pump cycle, no load-lock.
- Pressure adjustment via gas flow and/or rotational speed of the pump system.

Substrate handling:

- Substrate diameter of 100 mm respectively 4” wafer.
- Distance to target adjustable from 50 to 150 mm.
- Heating up to 600 °C.
- Bias option.
- Module/Assembly purchase.

Single cathode:

- 75 mm or 3” diameter target size.
- Unbalanced magnetron.
- Indirect cooling.
- Space for 6” cathode if possible.

General:

- Gas supply: Argon, Nitrogen, Acetylene.
- Relay control, operator safety ensured.
- Step by step process control. Operator fully responsible.

Die approbierte gedruckte Originalversion dieser Diplomarbeit ist an der TU Wien Bibliothek verfügbar
The approved original version of this thesis is available in print at TU Wien Bibliothek.
TU WIEN Bibliothek Your knowledge hub

- Plasma excitation via DC or Mid frequency (MF) power supplies.
- Bottom up design (sputter flux).
- Sputter shielding in the upper area.
- Overall low-cost design.

As the project progressed, some requirements for the system changed and demanded adjustments to the design. Especially due to an unforeseen damage of the magnetron sputtering system type Leybold Heraeus Z400 "Ylvi", the electrical design was developed in conjunction with the restoration of the system ident. Therefore, a switch cabinet and control concept were developed, which allows operating several recipients in plug and play. The development and manufacturing costs of two ident control cabinets were therefore supposed to be kept low.

The original wish to purchase the substrate heating could not be realized due to economic reasons. Therefore a design developed by Philipp Ertelthaler, mentioned in Zauner et al. [51], was adapted in size and integrated. In order to be able to equip the system with two cathodes in a later stage, the substrate rotation for uniform layers was also implemented. At the same time a uniform heating of the relatively large substrate holder by two lamps could be realized.

Furthermore, the request to operate the system as a HiPIMS system has arisen. A lot of scientific work underline the advantages in the production of DLC layers [2, 3, 52, 53]: higher ionization leads to higher sp^3 content, lower target poisoning and more stable and repeatable processes and higher density and hardness. However, the power supplies require more installation space than "usual" sputter power supplies. Therefore, it became necessary to create space for a generator in the machine frame after the switch cabinet was already in production and too small.

In the following chapters, the design of the sputtering system is discussed, in particular which decisions were made and how.

Die approbierte gedruckte Originalversion dieser Diplomarbeit ist an der TU Wien Bibliothek verfügbar
The approved original version of this thesis is available in print at TU Wien Bibliothek.
TU WIEN Bibliothek Your knowledge hub

5.1 Vacuum and Chamber Design

The layout of the vacuum design, including all associated components, was based on a wide variety of decisions. Starting with the chamber design, different variants of possible recipient shapes were investigated. Cylindrical, cubic and spherical contours were examined for advantages and disadvantages. The following aspects were considered and compared:

- Production and price.
- Surface/volume ratio.
- Possible accesses/openings for the user.
- Arrangement of instruments and measurements.

A spherical chamber was finally chosen. The favorable surface to volume ratio leads to vacuum-relevant advantages as well as a lower weight. The achievable base pressure and the time (t) required are directly related to the desorption rate (Q_{des}) and thus also to the area. Equation (5.1) shows this relationship, q_{des} is the specific desorption rate per area, t_0 is usually given as one hour. For cubic vacuum chambers, heavier wall thicknesses are necessary in addition to the large surface area, since flat surfaces deform more when pressure is applied (overpressure of the air pressure from outside). This must also be taken into account with the small maximum overpressure of 1 bar.

All flanges mounted normal to the surface point into the center of a spherical chamber. For example, a Langmuir probe for plasma analysis can easily be installed. A disadvantage, however, is the complicated realization of divisible, compact spherical chambers. Therefore, a variant with two quick access doors was chosen for the daily operations. For maintenance work three to four times a year, a large flange has to be loosened and dismantled.

Some suppliers of vacuum technology offer standardized vacuum chambers or even online tools for modification. However, the need of many large flanges and the installation of fixings for shielding have led to the development of the chamber completely own. A parameterized computer aided design (CAD) model was created to easily adapt the chamber to different semi-finished products from suppliers. A plane and axis system similar to a spherical coordinate system was introduced. Finally, three chambers with a diameter of 18", 400 mm and 403 mm were designed, see Figure 5.1a. Thus, quotes from three well-known manufacturers, including the required standard components, could be obtained. The contract was awarded both from an economic point of view and based on quality features.

TU Bibliothek Your knowledge hub WIEN
Die approbierte gedruckte Originalversion dieser Diplomarbeit ist an der TU Wien Bibliothek verfügbar
The approved original version of this thesis is available in print at TU Wien Bibliothek.

Furthermore, the supplier is located with a subsidiary in Vienna and has already supplied components for other systems. Therefore, short delivery times or stock goods can be expected for later modifications or maintenance. It is also possible to keep some identical spare parts in stock in the laboratory. In addition to the vacuum hardware, the pumping system and vacuum measurement technology was thus also purchased from the same manufacturer.

To achieve a basic pressure of less than 10^{-6} mbar different flange systems can be used. The simpler and cheaper variant would be with O-ring sealed flanges, so-called KF (German: Klein Flansch) or ISO-K/ISO-F flanges according to DIN 28403 [54] and DIN 28404 [55]. These are suitable in vacuum ranges up to 10^{-8} mbar due to the elastomer seals, as already described in chapter 2.2.3. The more expensive CF (Conflat) flanges, however, can also be used in UHV areas and are bake able to 450 °C [56]. The large number of flanges and the resulting large total area of elastomeric seals contributed to the decision to apply the copper-sealed CF system. Desorption on plastic surfaces is essentially related to the diffusion in the material, thus the desorption rate can be expressed with the diffusion rate (Q_{diff}). A_d is the surface of the elastomers in vacuum, q_{diff} is the area-specific diffusion density (see Equation (5.2)). In addition, permeation is a decisive factor, especially in the case of elastomer seals. The permeation flow (Q_{perm}) depends on the external pressure (p_a), d and the permeation constant (k_{perm}), according to Equation (5.3). More detailed descriptions and values for desorption, outgassing and permeation can be found in the literature [5, 6, 14]. Together with the leak rate (Q_L) (see Equation (5.4)) and the pumping speed, the achievable base pressure can be estimated (see Equation (5.5)) [5, 21].

$$Q_{des} = q_{des} \cdot A \cdot \frac{t_o}{t} \tag{5.1}$$

$$Q_{diff} = q_{diff} \cdot A_d \cdot \sqrt{\frac{t_0}{t}} \tag{5.2}$$

$$Q_{perm} = k_{perm} \cdot A \cdot \frac{p_a}{d} \tag{5.3}$$

$$Q_L = \frac{\Delta p \cdot V}{\Delta t} \tag{5.4}$$

$$Q_{des}(t) + Q_{diff}(t) + Q_{perm} + Q_L = p(t) \cdot S \tag{5.5}$$

Die approbierte gedruckte Originalversion dieser Diplomarbeit ist an der TU Wien Bibliothek verfügbar
The approved original version of this thesis is available in print at TU Wien Bibliothek.
TU Bibliothek WIEN Your knowledge hub

For vacuum generation, a two-stage pumping system with a turbomolecular pump and a two-stage rotary vane pump as backing pump was selected due to the already mentioned properties in chapter 2.3. As the system has to be flooded and opened after each coating process, relatively large pumps were selected to reach the base pressure fast. The turbo pump is started automatically via the relay control only after reaching a pressure of 1 mbar. To prevent a backflow of oil mist into the recipient or the turbo pump from the rotary vane pump, a foreline valve was installed. Several vacuum gauges were integrated for pressure measurement and monitoring. In addition, vacuum switches (VS) were installed to ensure safety for the user, more on this later. Figure 5.1b shows the vacuum design and the vacuum gauges are listed in Table 5.1 with their measurement principle and range.

Table 5.1: Vacuum gauges with working range and principle.

Abbr.	**Working principle**	**Working range**	**Notes**
VS	Mechanical diaphragm	setpoint 30 mbar	2 x for safety only
PCR	Pirani + capacitive diaphragm	$5 \cdot 10^{-5}$ - 1500 mbar	-
IKR	Cold cathode	10^{-9} - 10^{-2} mbar	Activated via PCR
CMR	Capacitive diaphragm	10^{-5} - 0.1 mbar	Secured via valve, for process control

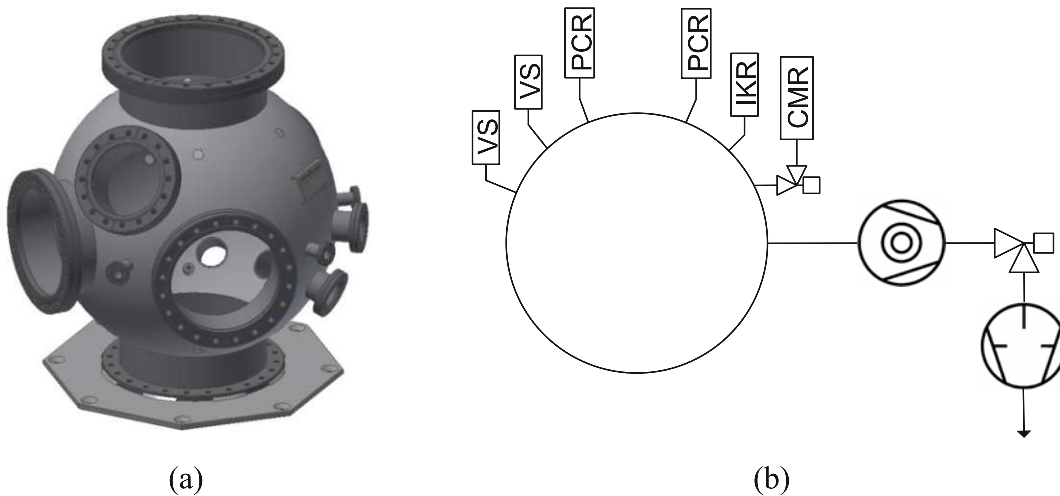

Fig. 5.1: (a) Vacuum chamber, (b) vacuum generation and pressure measurement design.

Die approbierte gedruckte Originalversion dieser Diplomarbeit ist an der TU Wien Bibliothek verfügbar
The approved original version of this thesis is available in print at TU Wien Bibliothek.
TU WIEN Bibliothek Your knowledge hub

A pressure control unit was installed in the switch cabinet to display the pressure of all vacuum gauges. In addition, six programmable set points can be relayed out via this control unit. The relays A to C are controlled by the measured pressure of the two PCRs. The relays A and B are integrated in the safety circuit of the acetylene supply. Relay C gives the release for the turbo pump. Switch points can be taken from the wiring diagram and must not be adjusted. To avoid contamination, the cold cathode ionization vacuum gauge (IKR) is switched on internally at sufficiently low pressure.

Die approbierte gedruckte Originalversion dieser Diplomarbeit ist an der TU Wien Bibliothek verfügbar
The approved original version of this thesis is available in print at TU Wien Bibliothek.
TU WIEN Bibliothek Your knowledge hub

5.2 Gas Distribution

For the reactive deposition of carbon layers respectively DLC layers, a hydrocarbon as carbon source is required in addition to argon as sputter gas. Acetylene (C_2H_2) was selected for the highest possible C/H ratio to achieve high possible carbon content in layers. However, due to its flammability and endothermic properties, this can only be handled under strict safety precautions, more on this later. In order to be able to use the system universally, a nitrogen supply was also implemented to sputter nitrides reactively. Oxides could be deposited if the acetylene supply is completely replaced by an oxygen supply due to safety aspects. The Figures 5.2 and 5.3 show the gas distribution panel and the main gas distribution scheme. The components are listed in Table 5.2, object numbers cross-reference the wiring diagram.

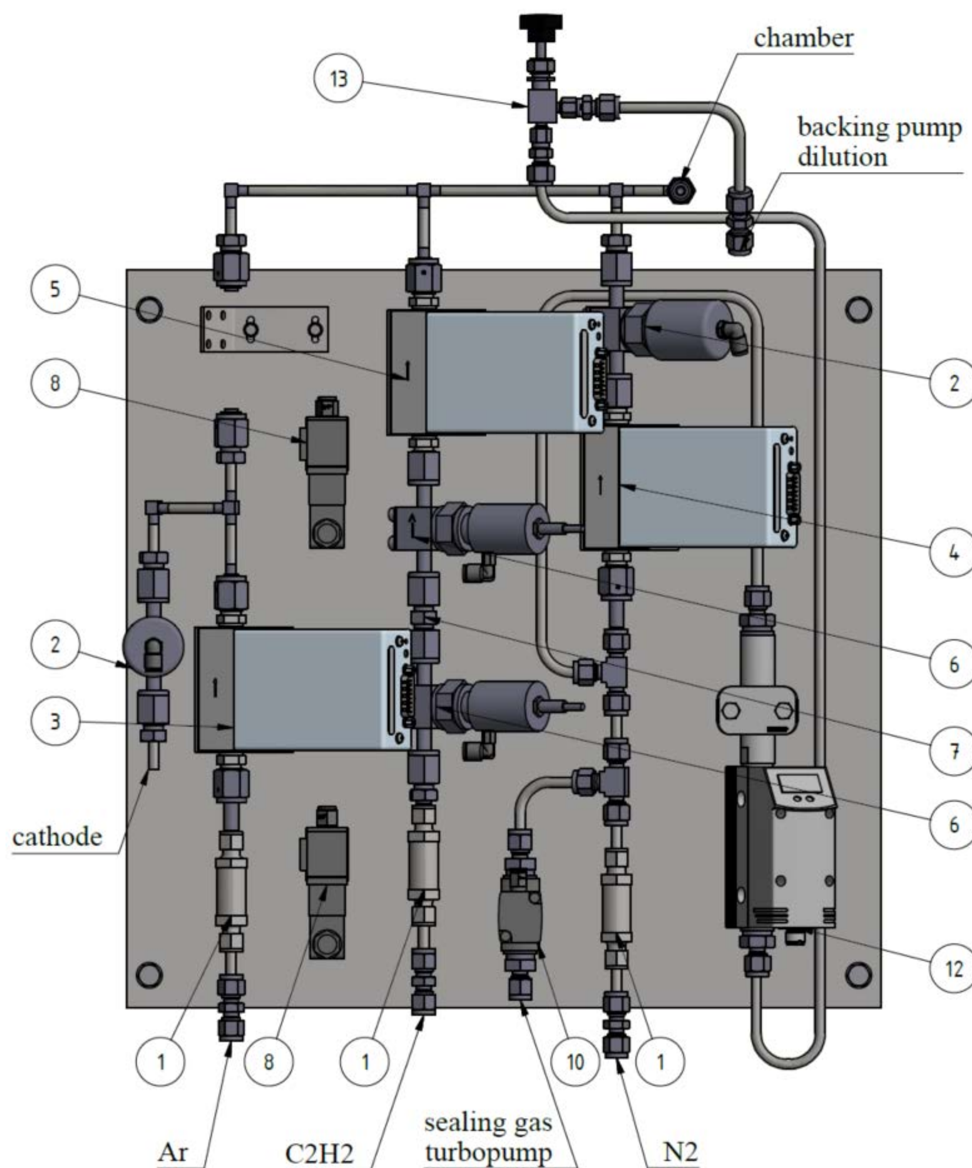

Fig. 5.2: Gas distribution panel.

Die approbierte gedruckte Originalversion dieser Diplomarbeit ist an der TU Wien Bibliothek verfügbar
The approved original version of this thesis is available in print at TU Wien Bibliothek.
TU WIEN Bibliothek Your knowledge hub

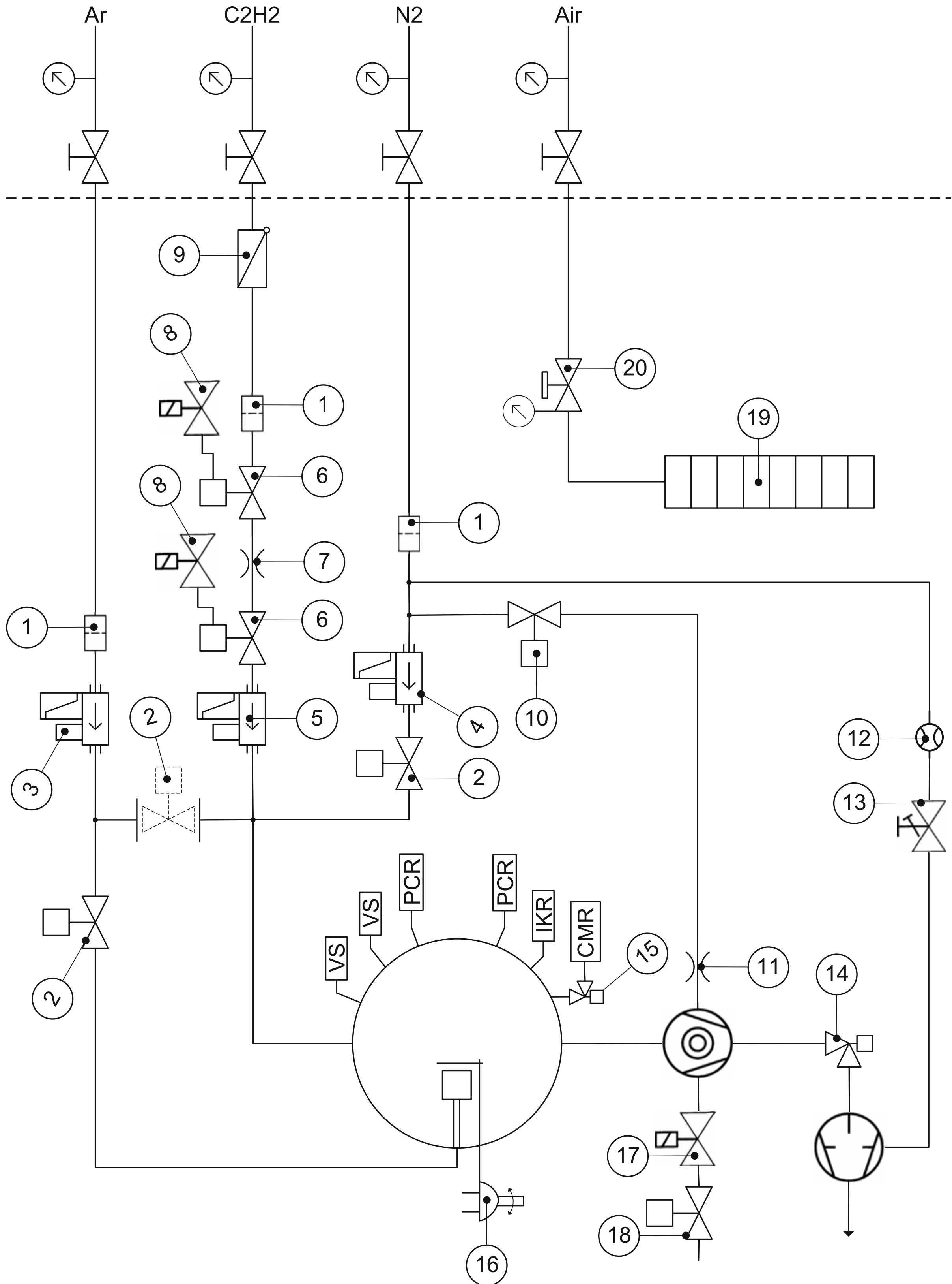

Fig. 5.3: Gas and compressed air distribution scheme.

Die approbierte gedruckte Originalversion dieser Diplomarbeit ist an der TU Wien Bibliothek verfügbar
The approved original version of this thesis is available in print at TU Wien Bibliothek.
TU WIEN Bibliothek Your knowledge hub

Table 5.2: Parts list of gas and compressed air distribution.

Nr.	Name	Object Nr.	Producer	#
1	Inline filter 7 µm	-	Fitok	3
2	Diaphragm valve	1103KK21/31	Swagelok	2
3	MFC for Ar	1103BF31	MKS	1
4	MFC for N_2	1103BF21	MKS	1
5	MFC for C_2H_2	1103BF11	MKS	1
6	Bellows sealed valve	1103KK11.1/2	Swagelok	2
7	Orifice VCR 50 µm	-	Lenox Laser	1
8	Solenoid valve	1103KK12.1/2	SMC	2
9	Flashback arrester	-	Linde Gas	1
10	Sealing gas valve	1143KK31	SMC	1
11	Orifice tube 30 µm	-	Lenox Laser	1
12	Flow rate meter N_2	1103BF51	IFM	1
13	Needle valve	-	Swagelok	1
14	Foreline valve	1143KK21	Pfeiffer Vacuum	1
15	UHV valve	1143KK11	VAT	1
16	Rotary actuator	1104KK01	SMC	1
17	Venting valve n.o.	-	Pfeiffer Vacuum	1
18	Flood valve	-	SMC	1
19	Valve terminal	1101A01	SMC	1
20	Filter/regulator	-	SMC	1

Thermal mass flow controllers (MFCs) (3-5) are used to regulate the gas flow. The measuring principle is based on the specific heat capacity and the different temperature profiles at different mass flows, explained in [5, 6, 57]. Integrated valves react and regulate to the set mass flow respectively the adjusted volume flow. The unit commonly used for the volume flow in these dimensions is standard cubic centimeters per minute [sccm]. According to DIN 1343 [58] 1 sccm corresponds to 1 cm^3/min of gas under standard conditions (0 °C and 1.013 bar). The selection of the MFCs was based less on economic factors. High accuracy and reproducibility were just as important as the possibility of being able to set the type of gas and working ranges within a certain limit. More details can be found in the manuals. Since the MFC series used is elastomer sealed, the C_2H_2-MFC had to be given special consideration. Ar and N_2 are inert and also C_2H_2 is also well compatible with most sealants. However, C_2H_2 is dissolved in acetone in pressure cylinders. This means that a considerable amount of acetone

TU Bibliothek Your knowledge hub WIEN
Die approbierte gedruckte Originalversion dieser Diplomarbeit ist an der TU Wien Bibliothek verfügbar
The approved original version of this thesis is available in print at TU Wien Bibliothek.

can enter the system, especially when the pressure cylinder is emptied below 5 bar of overpressure. As acetone is aggressive to some standard sealants, ethylene propylene diene monomer rubber (EPDM) sealants were used for this MFC.

All gases are fed into the system through a filter (1) and additional shut-off valves (2, 6). Ar is then directed into the system via the cathode. This has advantages in igniting and maintaining the plasma. However, there are some disadvantages for the sputter etching of substrates before the coating process. After Ar is introduced under the shutter of the target, the etching process must be run with relatively high gas flows. This can be easily observed by opening the target shutter during the etching process. The etching plasma becomes massively brighter. To counteract this effect the option of a second Ar valve was considered. If this valve is installed, Ar can be introduced into the chamber at the better position opposite the turbo pump, as N_2 and C_2H_2.

N_2 is fed into the chamber as a reactive gas, but it also fulfils other important functions as a clean inert gas within the system. During the coating process it is fed into the turbo pump as sealing gas to protect the engine and bearings from contamination. For this purpose, the sealing gas valve (10) is opened simultaneously with the gas valves (2, 6). To prevent damage and overpressure, an orifice (11) is required before the inlet into the turbo pump. A flow of 15 sccm may be introduced according to the manufacturer. For this purpose, a flow calibrated orifice with a diameter of 30 µm has been installed. However, the pressure of the N_2 supply line must be limited to 1.5 bar absolute (0.5 bar overpressure).

N_2 is also used to dilute the volume flow of C_2H_2 and thus prevent ignitable mixtures. For this purpose, a limited flow of C_2H_2 is mixed with N_2 before the pressure in the rotary vane pump is increased. The flow rate is adjusted via a shut-off and control valve (needle valve 13) and monitored by a flow meter (12). The N_2 is introduced via the gas ballast valve of the backing pump. Here too, the pressure of 0.5 bar overpressure must not be exceeded. The flow rate must not exceed 1260 l/h according to the operating instructions. According to DIN EN ISO 10156 [59], a content of 3 vol% C_2H_2 in the mixture with N_2 is no longer flammable in air. With a maximum of 50 sccm C_2H_2 flow, this result in a minimum N_2 flow of 1616.67 sccm or 1.62 l/min.

The C_2H_2 supply is specially protected due to the danger of explosion. Furthermore, C_2H_2 is chemically unstable and can explode even without air or oxygen [60]. Therefore it was important to deal with standards for explosion protection, mainly the DIN EN 1127 [61]. The risk assessment and later the reduction of risk to a minimum level through suitable design,

Die approbierte gedruckte Originalversion dieser Diplomarbeit ist an der TU Wien Bibliothek verfügbar
The approved original version of this thesis is available in print at TU Wien Bibliothek.
TU WIEN Bibliothek Your knowledge hub

technical safety precautions and its monitoring have taken on great importance. The C_2H_2 valves (6, and additionally 8) are only opened when all safety-relevant requirements for the prevention of explosive mixtures have been met. The function of the valves (6) is monitored additionally and an orifice (7) ensures that only a certain dilute-able quantity (50 sccm) is introduced into the system. All safety precautions are listed here:

- Machine doors are closed: monitored via safety switches.
- The backing pump is on and running: monitored via contactor and pressure switch.
- The foreline valve is opened: monitored via mechanical switch.
- The pressure in the system is below 1 mbar: double secured via two VS and two PCR; no dangerous situation can occur under vacuum condition, even if there are ignition sources.
- The dilution is sufficient: secured via the flow meter switch.
- The safety valves (6) open and close correctly: mechanical switches.

The operator is additionally responsible that the C_2H_2 gas cylinder is not emptied below 7 bar, that the pressure in the supply line does not exceed 0.5 bar overpressure and that the shut-off valve on the cylinder pressure reducer is only opened during the process. The leak tightness of the supply system must also be checked regularly. The flashback arrester (9) must be installed and checked at the designated intervals.

The pneumatic components are switched directly by the user with the use of a valve terminal (19) after the safety-relevant preconditions have been met. The pressure should be at least 4 bars to ensure the function of all valves, and a maximum of 7 bars is permitted. The pressure regulator (20) must be set accordingly. The valves 2, 6, 10, and 14 already described are switched pneumatically. In addition, the CMR is protected against atmosphere and contamination by a UHV angle valve (15). The rotary drive of the target shutter is pneumatically operated and the flood valve (18) is closed pneumatically, simultaneously with the opening of the foreline valve. The second flood valve (17) is closed as soon as the turbo pump is supplied with power and opens automatically with a delay when the pumping station is switched off.

TU Bibliothek WIEN Your knowledge hub
Die approbierte gedruckte Originalversion dieser Diplomarbeit ist an der TU Wien Bibliothek verfügbar
The approved original version of this thesis is available in print at TU Wien Bibliothek.

5.3 Electrical design and safety

For the operation of a PVD system a multitude of devices and sensors are necessary. These can be divided into the following functional groups: vacuum, process gas, process, safety, heating, cooling water, and substrate movement (see Table A.1).

The following paragraphs briefly describe which at first glance invisible circuits in the background contribute to the functioning of the system and safety. The complete documentation in form of a wiring diagram can be found at the system and at the institute and is not integrated in this thesis due to its large extent. However, the object numbers used refer to it. For a later use of the same concept for another PVD system, some possible extensions have already been functionally implemented, but not built in. These are: the operation of a second cathode and thus a 3rd sputter generator and the extension by a load-lock. A 3rd DC power supply was already installed within the project to superimpose a DC and HiPIMS signal via a diode module. In order to be able to supply another recipient with the same control cabinet, a plug and play system was implemented. A connection box was installed in the machine frame for this purpose. The signals and power are transmitted via 2 x 64 pin and 24 pin cables and connectors respectively.

5.3.1 General structure

The system is supplied with 2 x 32 A/400 VAC. The main switch is also an emergency stop switch and sets the system into a safe state. The supply voltage is divided between the generators, the 230 VDC supply and the 24 VDC supply. In accordance with their requirements, all devices are protected by circuit breakers. These are accessible at the front of the switch cabinet. Safety circuits are activated by contactors; dangerous circuits are protected by two contactors. These are checked when the system is switched on via the main switch. Illuminated switches indicate to the user whether this device, valve or function may be activated. Flashing switches mean a safety-relevant deactivation of functions. To repair or eliminate faults, the system must be switched off via the main switch. When turned on again, a reset and a new initial check is performed.

5.3.2 Safety

The security functions are essentially divided into two areas: Machine safety and user safety. The former is implemented via simple circuit breakers. Additionally, to avoid improper operating conditions and damage, the cooling water is monitored and some process conditions

Die approbierte gedruckte Originalversion dieser Diplomarbeit ist an der TU Wien Bibliothek verfügbar
The approved original version of this thesis is available in print at TU Wien Bibliothek.
TU WIEN Bibliothek Your knowledge hub

are integrated into the machine safety circuits. The user safety is SIL 2 certified (safety integrity level) according IEC 62061 [62] and includes the following aspects: protection against high electrical voltages; protection from hot surfaces; avoidance of ignitable mixtures and thus explosion protection.

Machine safety ensures that sensitive components are only used in the appropriate ranges. The turbo pump requires a backing vacuum for proper operation. For this purpose, the contactor is only released when the backing pump is switched on and a vacuum of less than 1 mbar is reached. The pressure switching point is provided by the measurement of a PCR and a relay of the vacuum gauge control. In addition, the turbo pump must be cooled. The cooling water supply is divided into the circuits for the cathode (the magnetron) and the second circuit for the turbo pump, substrate heating and the rotary feedthrough. The inflow and the two returns are flow monitored. Reaching of the threshold is visually indicated by the green display on the controllers. The switching points of the relays activate the control of the turbo pump. If the contactor is activated, the substrate heating can also be enabled and a relay releases the interlocks of the sputter generators. After turning on the backing pump, the user can also open the foreline valve, the UHV valve for the capacitive diaphragm gauge and the gas valves for argon and nitrogen. To protect the bearings and the motor of the turbo pump, the purge gas is opened at the same time as the gas valves.

The **user safety** is even more complex. The doors of the machine frame must be closed for any operation. The front door is additionally locked to prevent operator mistakes during processing. Inside the vacuum chamber there are the following hazards: dangerous voltages from the sputter generators, high temperatures of the substrate heating and rotating parts. In addition, there is a potentially explosive atmosphere due to the acetylene stream. Under vacuum, it is ensured that neither the user can touch dangerous parts in the vacuum chamber, nor that the ignitable mixture can lead to explosions. For this reason, safety-certified vacuum switches have been installed which enable the functions just described at a switching point of 30 mbar. Since the processes run at much lower pressures anyway, it was decided to set additional switching points at a pressure of 1 mbar using two PCRs and the pressure control unit.

The last dangerous point is the acetylene flowing in and out. The inflow is doubly secured by two process valves and two upstream solenoid valves. The function of the process valves is checked by position sensors. These valves can only be switched if additional conditions are fulfilled: The gas must be able to flow out unhindered, i.e. the backing pump must be running

Die approbierte gedruckte Originalversion dieser Diplomarbeit ist an der TU Wien Bibliothek verfügbar
The approved original version of this thesis is available in print at TU Wien Bibliothek.
TU Bibliothek WIEN Your knowledge hub

and the foreline valve must be open. An additional sensor is installed on the rotary vane pump and a position indicator is integrated in the angle valve. On the outlet side, the acetylene is rendered incombustible by the nitrogen dilution already mentioned. If a sufficient flow rate is also set here, the safety valves can be opened. Of course, they close automatically before an unsafe condition arises again.

Die approbierte gedruckte Originalversion dieser Diplomarbeit ist an der TU Wien Bibliothek verfügbar
The approved original version of this thesis is available in print at TU Wien Bibliothek.
TU WIEN Bibliothek Your knowledge hub

5.4 Substrate handling

For the economic reasons already mentioned, the substrate heating, including rotation, z-shift, cooling and bias supply, was designed and built in-house. A commonly used concept of heating with powerful light bulbs was adapted for this purpose, see Figure 5.4. Two 1000 W light bulbs (1) are mounted in a lamp housing (2) with ceramic enclosures (3) containing the connection pins. Special Kapton insulated UHV suitable cables were used to supply the lamps. Protected behind quartz glass (4), part of the heating power is thus transmitted to the back plate (5) of the substrate holder (6) mainly via infrared radiation. The back plate should distribute the heat uniformly. The rest of the heat is transferred to the lamp housing, thus requiring cooling.

The temperature is measured by a type K sheathed thermocouple (7) with fiber optic cable inside the lamp housing. It is complex and expensive to implement a contactless temperature measurement in vacuum directly on the rotating substrates. Therefore it was necessary to record calibration curves which show the different temperature rise of the lamp housing and the substrate, see appendix B, Figures B.1, B.2, and B.3. The cooling is achieved by cooling channels (8) of a welded-on cooling body at the rear of the housing. Flexible stainless-steel corrugated hoses connected with face sealed fittings (9) supply cooling water. A rotating shaft (10) simultaneously supplies the substrate holder with bias voltage. The shaft is shielded electrically and thermally by ceramic tubes (11), as well as the thermocouple. The substrate holder is attached to the shaft without tools via a bayonet.

A lifting mechanism was developed to realize a z-shift of 100 mm, see Figure 5.5. A CF-sealed diaphragm bellow (1) is expanded or compressed between a base plate (2) and a slide (3). At the top part (4) are the drive (5) and the bearing (6) of the trapezoidal threaded lead screw (7) and the position indicator (8). Linear bushings (9) enable a stable parallel stroke over the axes (10). Special attention has been paid to tolerances and bending in this assembly, as there is not much space between the bellows and the through fixture for the heater. A force of 227 N is exerted on the slide due to vacuum and the force required stretching the bellow plus 128 N due to the weight of the assembly loaded. A simplified mechanical stress analysis was performed directly in the CAD-tool. The mechanically loaded parts were made more massive to avoid collisions during operation and damage of the pretty expensive bellow.

Die approbierte gedruckte Originalversion dieser Diplomarbeit ist an der TU Wien Bibliothek verfügbar
The approved original version of this thesis is available in print at TU Wien Bibliothek.
TU WIEN Bibliothek Your knowledge hub

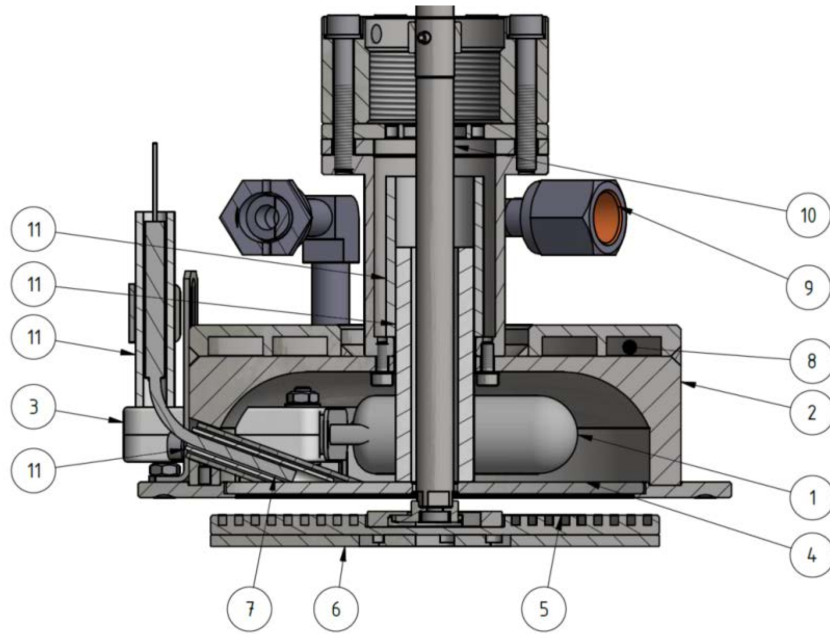

Fig. 5.4: Substrate heater assembly.

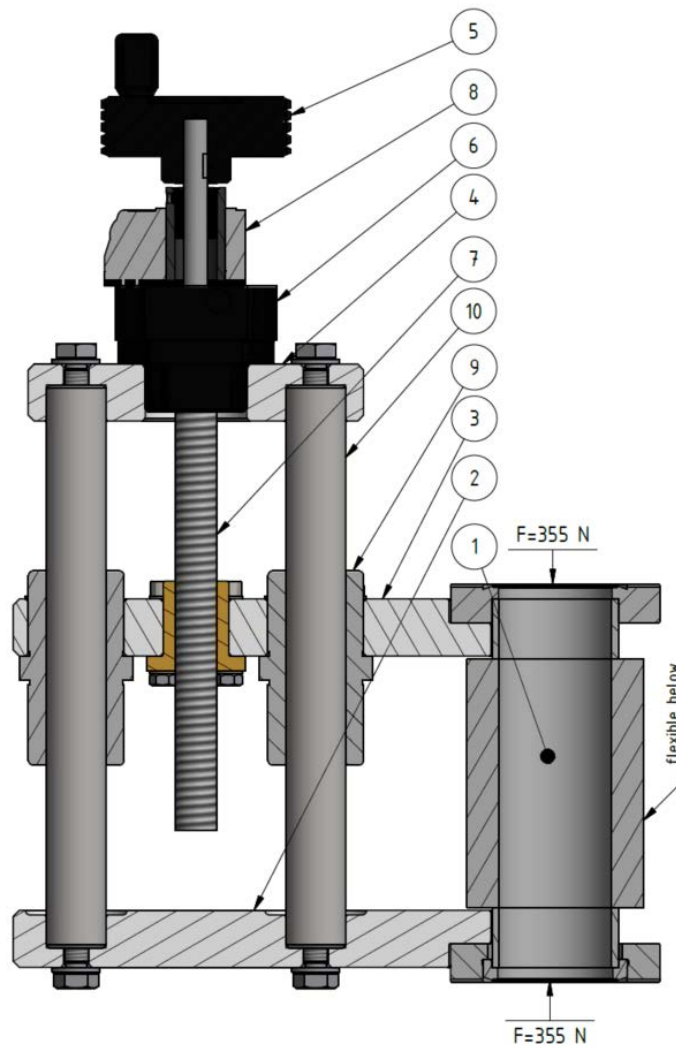

Fig. 5.5: Lifting mechanism with diaphragm bellow (1).

Die approbierte gedruckte Originalversion dieser Diplomarbeit ist an der TU Wien Bibliothek verfügbar
The approved original version of this thesis is available in print at TU Wien Bibliothek.
TU WIEN Bibliothek Your knowledge hub

The drive of the substrate rotation and the bias supply is shown in Figure 5.6. The substrate rotation is driven by a 24 VDC gear motor (1) which allows a speed of up to 85 rpm controlled by a potentiometer. The bias power is transmitted in a specially designed, fully separable POM housing (6) via sliding contacts (5) to a collector ring (4). The engine is therefore connected to the transmission line via a non-conductive POM shaft (3) and a separable claw coupling (2). The bias voltage (blue line) is transmitted through the shaft of the UHV rotary feedthrough (7), the stainless-steel bellow coupling (9) and then to the substrate shaft (11). Therefore, the rotary feedthrough is also at bias potential and is separated from ground by the POM tube (8) and an UHV insulator (12). The coupling and shaft are isolated in vacuum by PEEK housings (12, 13) and PEEK bearing seats (14). The holder for the lamp housing (15) is screwed between the lower flange of the UHV insulator, the upper flange of the corrugated bellow (16) and the slide of the lifting mechanism (17).

More detailed drawings of the assemblies and the individual parts can be found in the documentation at the institute. Due to the large amount and the large paper formats, these cannot be published in this thesis. The same applies to parts lists.

Die approbierte gedruckte Originalversion dieser Diplomarbeit ist an der TU Wien Bibliothek verfügbar
The approved original version of this thesis is available in print at TU Wien Bibliothek.
TU Wien Bibliothek Your knowledge hub

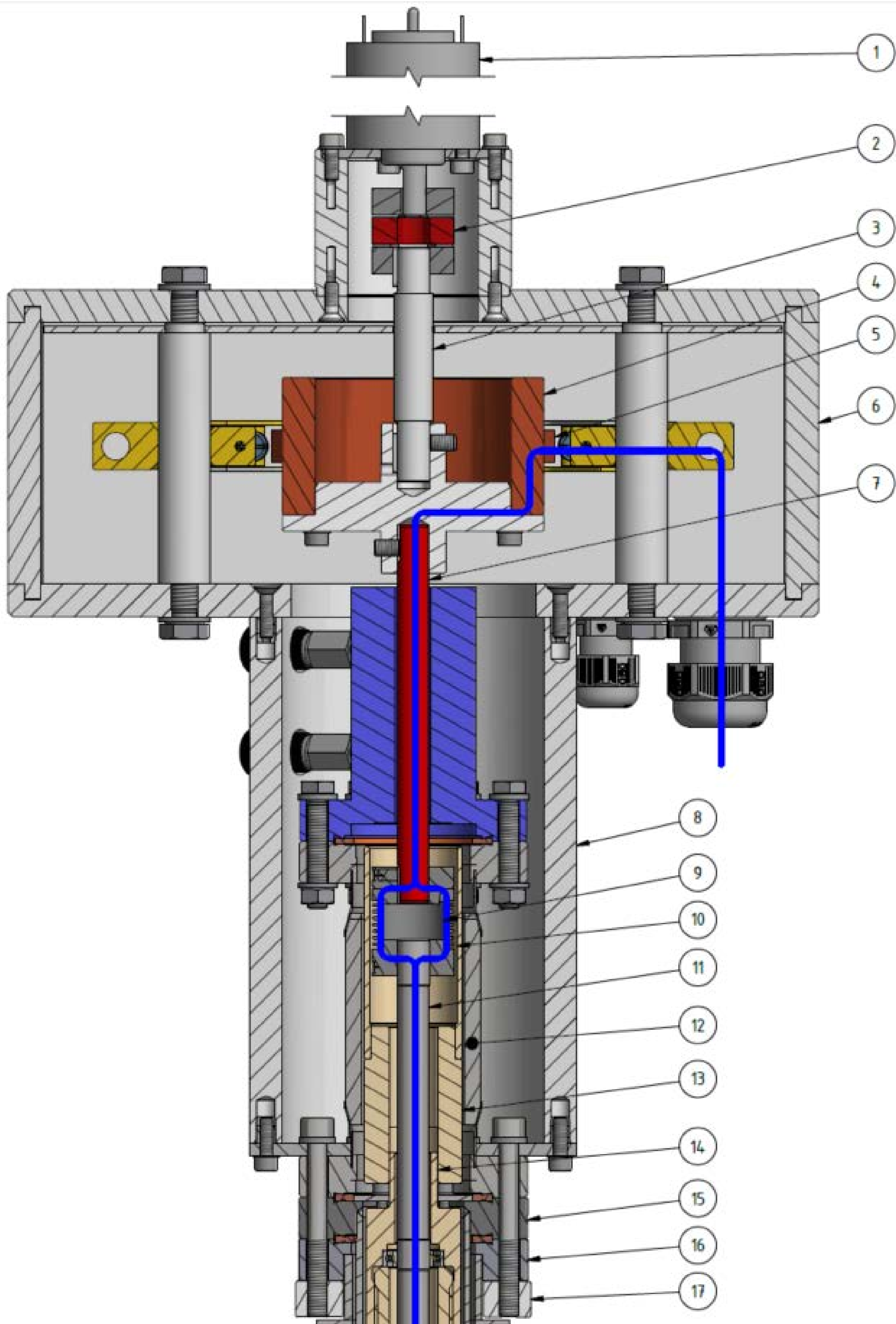

Fig. 5.6: Rotary drive and bias supply (blue line) of the substrate.

Die approbierte gedruckte Originalversion dieser Diplomarbeit ist an der TU Wien Bibliothek verfügbar
The approved original version of this thesis is available in print at TU Wien Bibliothek.
TU WIEN Bibliothek Your knowledge hub

5.5 Magnetron

For the acquisition of the magnetron (commonly called cathode), a manufacturer was chosen who already supplies magnetrons or single magnet systems for other PVD systems. The requirements have already been described in the beginning of chapter 5. For Frida a new design was purchased that allows the user to change the target even if there is little space inside the chamber. Only the screw of the shutter has to be loosened with a tool to be able to remove the anode wall. Then the target can be fixed by a large target nut with fine thread. Since this magnetron is built to use targets with 75 mm as well as 3" diameter, a well centered installation is necessary due to the large tolerance. The production of centering rings for smaller targets or a nut with a smaller bore would be an option at a later stage. The magnetron can be adjusted in height with the long shaft. This is not necessary and intended for normal use, but may be helpful to coat larger components. In this case, care must be taken to ensure that the seals of the feedthrough are clean. The original height can be readjusted via the substrate position indicator. In Figure 5.7 the magnetron is shown at the initial installation.

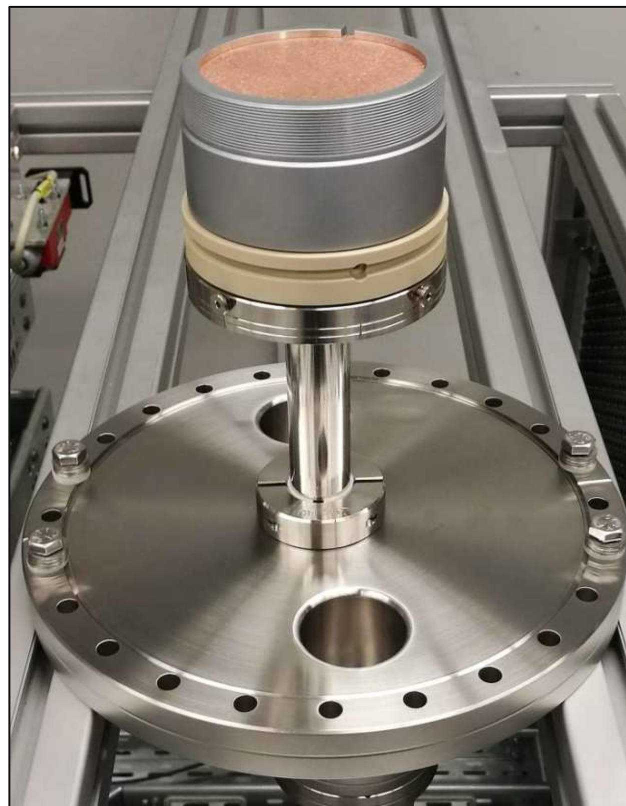

Fig. 5.7: Unbalanced circular magnetron.

Die approbierte gedruckte Originalversion dieser Diplomarbeit ist an der TU Wien Bibliothek verfügbar
The approved original version of this thesis is available in print at TU Wien Bibliothek.
TU WIEN Bibliothek Your knowledge hub

5.6 Machine frame and cooling water

For cost reasons, the machine frame on Figure 5.8 was not constructed as a solid welded assembly, but as an assembly with aluminum construction profiles. Since a very compact design was desired, it was tried to construct as detailed as possible. This also included cable ducts. The front door (1) gives access to the rotary vane pump, magnetron, gas and compressed air distribution. On the right front side there is a 19" rack (2), which was added for the installation of the HiPIMS generator and an industrial PC.

Through the rear door (3) one gets access to the diode module and the connections of the HiPIMS generator and the industrial PC. In addition, on the rear side there is the cable box (4), into which all devices are wired and which also contains the valve terminal. Below this is the cooling water supply (5). The actuators (6) for the safety switches are also mounted on the doors.

Die approbierte gedruckte Originalversion dieser Diplomarbeit ist an der TU Wien Bibliothek verfügbar
The approved original version of this thesis is available in print at TU Wien Bibliothek.
TU WIEN Bibliothek Your knowledge hub

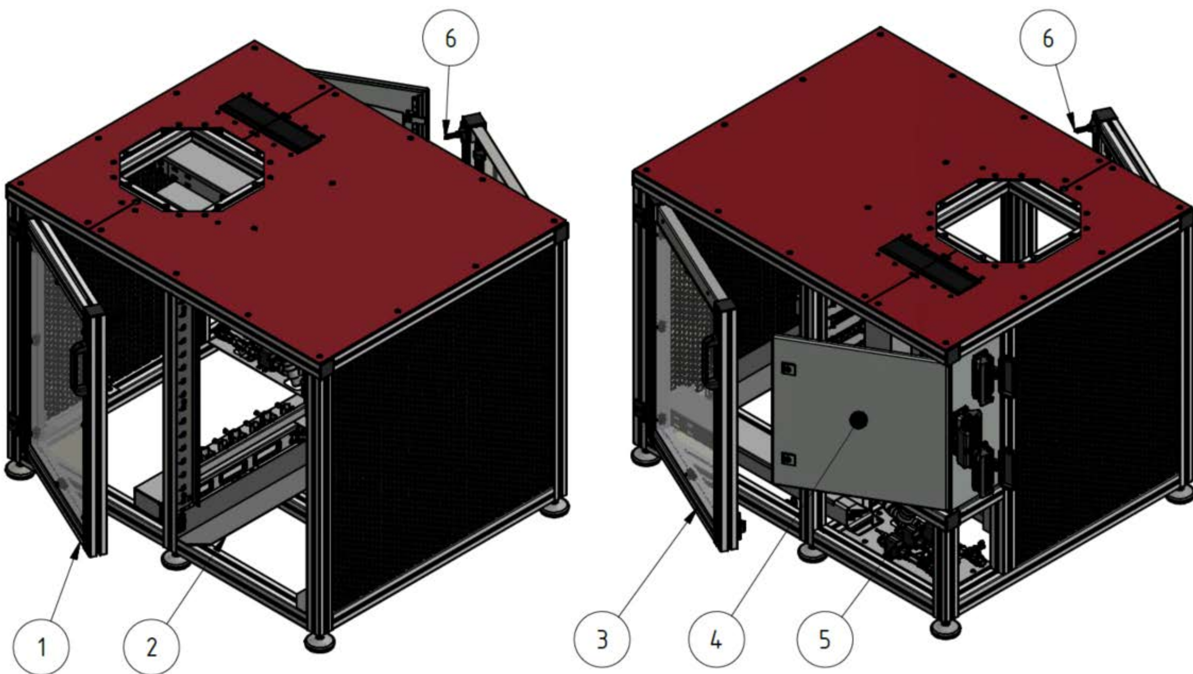

Fig. 5.8: Machine frame.

The **cooling water supply** (Figure 5.9) consists of three ball valves for the inlet (1), the outlet (2) and the drain (3). The filter (4) protects the devices and the flow and temperature sensors (5) transmit the signal to the display unit in the switching cabinet. With the pressure limiter (6) overpressure is prohibited. It is set to 3 bars due to the thin copper membrane in the magnetron.

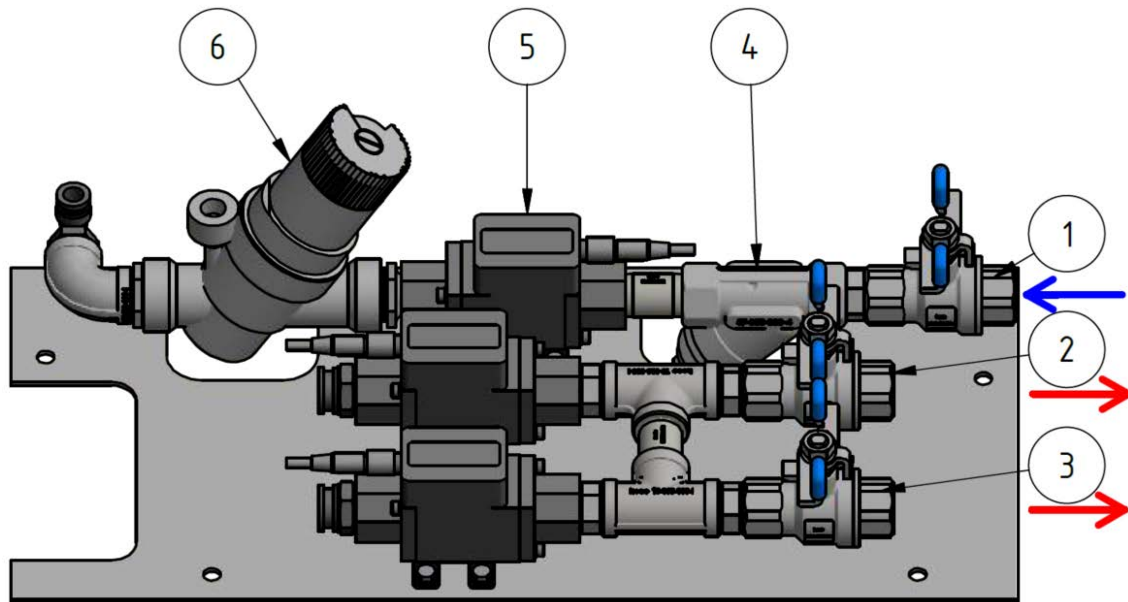

Fig. 5.9: Cooling water assembly.

Die approbierte gedruckte Originalversion dieser Diplomarbeit ist an der TU Wien Bibliothek verfügbar
The approved original version of this thesis is available in print at TU Wien Bibliothek.
TU WIEN Bibliothek Your knowledge hub

5.7 Operation

The safety circuits in the background only affect the user in case of unsafe situations and the following shutdown of the hazard sources. In order to operate the system and to deposit thin films, the user must initiate and monitor most of the necessary steps himself. He must therefore understand the process. However, he can then operate “Frida” (see Figure C.1) very easily in just a few steps. A typical coating process works as follows:

- Start of the pumping system.
- Opening the foreline valve.
- The turbo pump starts automatically below 1 mbar.
- Waiting until the base pressure is sufficient. About $2 \cdot 10^{-6}$ after 1.5 hours.
- The cold trap (cold finger) can improve the performance.
- The chamber heater helps to achieve a lower base pressure, especially if the chamber has been exposed to air for a long time.
- The shut-off valve of the process pressure gauge (CMR) is opened.
- The substrate heating and thus the rotation must be set and started about 20 minutes before the process starts. The calibration curves are given in appendix B.
- The gas flow is adjusted by a control unit on the control cabinet.
- The process pressure is also set with the gas flow. In addition, the speed of the turbo pump can be reduced.
- The target shutter protects the target from contamination during sputter cleaning and is opened at the start of the process.
- The sputter generators and the bias voltage are set and started according to the desired process.
- The plasma can be observed through the viewing window.
- The temperature of the cooling water of the cathode can be observed at the control cabinet.
- After the process the generators are switched off and the gas valves are closed (also the MFC's).
- The substrate heating is switched off.
- Waiting until the substrate has cooled down, at least 1.5 hours until the heater indicates below 60 °C.
- Turn of the substrate rotation.

Die approbierte gedruckte Originalversion dieser Diplomarbeit ist an der TU Wien Bibliothek verfügbar
The approved original version of this thesis is available in print at TU Wien Bibliothek.
TU WIEN Bibliothek Your knowledge hub

- Closing of the CMR shut-off valve before venting.
- Closing of the foreline valve.
- Turn off the pumping system; the chamber is vented automatically after a few seconds trough the turbo pump.
- The quick access doors can be opened
- The possibly charged target or substrate must be touched with the discharge lance.
- The samples can be taken out.
- To exchange the target, the cooling water must be turned off.

Die approbierte gedruckte Originalversion dieser Diplomarbeit ist an der TU Wien Bibliothek verfügbar
The approved original version of this thesis is available in print at TU Wien Bibliothek.
TU WIEN Bibliothek Your knowledge hub

5.8 Outlook

The system is designed for simple use to quickly carry out scientific experiments. However, it should be mentioned here how the possibilities and results of the plant can be improved in the future.

Especially for DLC coatings it is of crucial importance to evaluate the adhesion on many different substrates. Interlayers are often used for this purpose. To deposit these layers directly before the DLC layer, a second cathode is necessary. The system is already prepared for this purpose. The connection flange of the cathode has to be exchanged and two tilt able cathodes have to be installed. For the interlayer, a smaller cathode with a diameter of 50 mm or 2" would also be feasible and easier to implement in terms of space.

The plant is not equipped with pressure control due to cost pressure. The user is responsible for the etching and coating pressure via the set gas flow and possibly by reducing the rotational speed of the turbo pump. This leads to longer lasting undefined pressures, especially between the etching and coating process. For this reason, it is recommended at this point to install a pressure control valve between the recipient and the turbo pump.

Die approbierte gedruckte Originalversion dieser Diplomarbeit ist an der TU Wien Bibliothek verfügbar
The approved original version of this thesis is available in print at TU Wien Bibliothek.
TU Bibliothek WIEN Your knowledge hub

6 List of Figures

Fig. 2.1: Cube and particle movement to determine the pressure 4

Fig. 2.2: Stainless steel in vacuum technology 9

Fig. 2.3: Classification of vacuum pumps 12

Fig. 2.4: Common working ranges of vacuum pumps 13

Fig. 2.5: Working principle of rotary vane pumps 15

Fig. 2.6: Working principle of diaphragm pumps 16

Fig. 2.7: Working principle of screw pumps 17

Fig. 2.8: (a) Working principle and (b) compression ratio of roots pumps 18

Fig. 2.9: Working principle of claw pumps 19

Fig. 2.10: Blade geometry of turbomolecular pumps 21

Fig. 2.11: Theoretical working ranges of direct and indirect measurement principles. 22

Fig. 2.12: Working principle of (a) capacitive vacuum gauge and (b) piezo resistive vacuum gauge 23

Fig. 2.13: Pirani vacuum gauge curves for calibration 24

Fig. 3.1: Thin film deposition techniques 26

Fig. 3.2: (a) structure of glow discharge in PVD sputter systems; (b) sputter yield 28

Fig. 3.3: Balanced (left) and unbalanced magnetron (right) 30

Fig. 3.4: Structure zone diagram by A. Anders 32

Fig. 4.1: Ternary phase diagram of DLC films assuming sp^2 and sp^3 hybridized carbon and H to form DLC coatings 34

Fig. 4.2: Effect of humidity on COF: H-free and hydrogenated DLC films 35

Fig. 5.1: (a) Vacuum chamber, (b) vacuum generation and pressure measurement design. ... 40

Fig. 5.2: Gas distribution panel. 42

Fig. 5.3: Gas and compressed air distribution scheme. 43

Die approbierte gedruckte Originalversion dieser Diplomarbeit ist an der TU Wien Bibliothek verfügbar
The approved original version of this thesis is available in print at TU Wien Bibliothek.
TU Bibliothek Your knowledge hub WIEN

Fig. 5.4: Substrate heater assembly. 51

Fig. 5.5: Lifting mechanism with diaphragm bellow (1). 51

Fig. 5.6: Rotary drive and bias supply (blue line) of the substrate. 53

Fig. 5.7: Unbalanced circular magnetron. 54

Fig. 5.8: Machine frame. 55

Fig. 5.9: Cooling water assembly. 56

Fig. B.1: Temperature curve at maximum power. III

Fig. B.2: Temperature curve with set points in 50 °C steps. IV

Fig. B.3: Calibration curve of the substrate heater and recommended heater set points IV

Fig. C.1: Frida built up. V

Die approbierte gedruckte Originalversion dieser Diplomarbeit ist an der TU Wien Bibliothek verfügbar
The approved original version of this thesis is available in print at TU Wien Bibliothek.
TU WIEN Bibliothek Your knowledge hub

7 List of Tables

Table 2.1: Pressure regimes and their characteristics 7

Table 4.1: Typical properties of diamond, DLC coatings and graphite 34

Table 5.1: Vacuum gauges with working range and principle. 40

Table 5.2: Parts list of gas and compressed air distribution. 44

Table A.1: Devices, components, sensors and valves for the operation of the PVD system. I

Die approbierte gedruckte Originalversion dieser Diplomarbeit ist an der TU Wien Bibliothek verfügbar
The approved original version of this thesis is available in print at TU Wien Bibliothek.
TU WIEN Bibliothek Your knowledge hub

8 References

[1] K. Bewilogua, D. Hofmann, Surface and Coatings Technology 242 (2014) 214–225.

[2] T. Konishi, K. Yukimura, K. Takaki, Surface and Coatings Technology 286 (2016) 239–245.

[3] P. Souček, J. Daniel, J. Hnilica, K. Bernátová, L. Zábranský, V. Buršíková, M. Stupavská, P. Vašina, Surface and Coatings Technology 311 (2017) 257–267.

[4] DIN 28400-1:1990-05, Vakuumtechnik; Benennung und Definitionen; Allgemeine Benennungen, Beuth Verlag GmbH, Berlin, 1990.

[5] K. Jousten (Ed.), Handbook of vacuum technology, 2nd ed., Wiley-VCH Verlag GmbH & Co. KGaA, Weinheim, 2016.

[6] J.F. O'Hanlon, A User's Guide to Vacuum Technology, 3rd ed., John Wiley & Sons, Inc, Hoboken, NJ, USA, 2003.

[7] K. Wasa, I. Kanno, H. Kotera, Handbook of sputter deposition technology: Fundamentals and applications for functional thin films, nano-materials and MEMS, 2nd ed., Elsevier/Andrew, Amsterdam u. a., 2012.

[8] M. Knudsen, Ann. Phys. 333 (1909) 75–130.

[9] W. Jorisch (Ed.), Vacuum technology in the chemical industry, Wiley-VCH Verlag GmbH & Co. KGaA, Weinheim, Germany, 2015.

[10] A.P. Thompson, S.J. Plimpton, W. Mattson, The Journal of chemical physics 131 (2009) 154107.

[11] DIN EN 10088-1:2014-12, Nichtrostende Stähle - Teil 1: Verzeichnis der nichtrostenden Stähle, Beuth Verlag GmbH, Berlin, 2014.

[12] Y.H. Shin, K.J. Lee, K.C. Jhung, Vacuum 47 (1996) 679–682.

[13] C. Geyari, Vacuum 26 (1976) 287–297.

[14] D.M. Hoffmann, B. Singh, J.H. Thomas, Handbook of vacuum science and technology,

TU WIEN Bibliothek Your knowledge hub
Die approbierte gedruckte Originalversion dieser Diplomarbeit ist an der TU Wien Bibliothek verfügbar
The approved original version of this thesis is available in print at TU Wien Bibliothek.

Academic Press; Elsevier e-books, San Diego, 2014.

[15] D.G. Butomo, N.I. Zedin, O.S. Mnushkin, Met Sci Heat Treat 10 (1968) 184–185.

[16] L. de Chernatony, Vacuum 27 (1977) 605–609.

[17] R.N. Peacock, Journal of Vacuum Science and Technology 17 (1980) 330–336.

[18] K. Jousten (Ed.), Handbuch Vakuumtechnik, 12th ed., Springer Reference Technik, Springer Vieweg, Wiesbaden, 2018.

[19] DIN 28400-2:1980-10 Vakuumtechnik; Benennungen und Definitionen, Vakuumpumpen, Beuth Verlag GmbH, Berlin, 1980.

[20] DIN ISO 21360-1:2016-09, Vakuumtechnik - Standardverfahren zur Messung der Leistungsdaten von Vakuumpumpen - Teil 1: Grundlegende Beschreibung, Beuth Verlag GmbH, Berlin, 2016.

[21] The Vacuum Technology Book: Part 2, Pfeiffer Vacuum GmbH, Asslar, 2013.

[22] F.J. Eckle, P. Bickert, R. Lachenmann, Vacuum 46 (1995) 793–796.

[23] C.-F. Hsieh, Y.-W. Hwang, Z.-H. Fong, Mechanism and Machine Theory 43 (2008) 812–828.

[24] J. Wang, D. Cui, X. Pang, H. Feng, Z. Wang, Vacuum 143 (2017) 174–184.

[25] DIN IEC 60381-1:1985-11, Analoge Signale für Regel- und Steueranlagen; Analoge Gleichstromsignale, Beuth Verlag GmbH, Berlin, 1985.

[26] DIN IEC 60381-2:1980-06, Analoge Signale für Regel- und Steueranlagen; Teil 2: Analoge Gleichspannungssignale, Beuth Verlag GmbH, Berlin, 1980.

[27] G. Bräuer, in: S. Hashmi, G.F. Batalha, C.J. van Tyne, B.S. Yilbas (Eds.), Comprehensive materials processing, Elsevier, Oxford, Walltham, MA, 2014, pp. 57–73.

[28] P.M. Martin (Ed.), Handbook of Deposition Technologies for Films and Coatings (Third Edition), William Andrew Publishing, Boston, 2010.

[29] D.M. Mattox (Ed.), Handbook of Physical Vapor Deposition (PVD) Processing (Second Edition), Elsevier, Boston, 2010.

[30] M. Ohring (Ed.), Materials Science of Thin Films: Deposition and Structure, 2nd ed., Academic Press, San Diego, 2002.

[31] W.D. Sproul, Surface and Coatings Technology 49 (1991) 284–289.

Die approbierte gedruckte Originalversion dieser Diplomarbeit ist an der TU Wien Bibliothek verfügbar
The approved original version of this thesis is available in print at TU Wien Bibliothek.
TU Wien Bibliothek Your knowledge hub

[32] P.H. Mayrhofer, C. Mitterer, L. Hultman, H. Clemens, Progress in Materials Science 51 (2006) 1032–1114.

[33] B.A. Movchan, A.V. Demchishin, Fiz. Metal. Metalloved. 28: 653-60 (1969).

[34] P.B. Barna, M. Adamik, Thin Solid Films 317 (1998) 27–33.

[35] J.A. Thornton, Journal of Vacuum Science and Technology 11 (1974) 666–670.

[36] R. Messier, A.P. Giri, R.A. Roy, Journal of Vacuum Science & Technology A: Vacuum, Surfaces, and Films 2 (1984) 500–503.

[37] A. Anders, Thin Solid Films 518 (2010) 4087–4090.

[38] I. Petrov, P.B. Barna, L. Hultman, J.E. Greene, Journal of Vacuum Science & Technology A: Vacuum, Surfaces, and Films 21 (2003) S117-S128.

[39] K. Bobzin, Oberflächentechnik für den Maschinenbau, Master, 2013, http://lib.myilibrary.com/Open.aspx?id=525168.

[40] VDI 2840; Kohlenstoffschichten; Grundlagen, Schichttypen und Eigenschaften, Beuth Verlag GmbH, Berlin, 2012.

[41] J. Robertson, phys. stat. sol. (a) 205 (2008) 2233–2244.

[42] A. Erdemir, Surface and Coatings Technology 146-147 (2001) 292–297.

[43] M. Nakamura, Y. Takagawa, K.-i. Miura, J. Kobata, W. Zhu, N. Nishiike, K. Arao, E. Marin, G. Pezzotti, Diamond and Related Materials 90 (2018) 214–220.

[44] M. Nakamura, H. KODAMA, K.-i. Miura, K. DEMIZU, D. IBA, I. MORIWAKI, JAMDSM 6 (2012) 121–130.

[45] DIN 4855:2015-09, Kohlenstoffschichten - DLC-Schichten - Beschreibung der Schichtarchitektur, Beuth Verlag GmbH, Berlin, 2015.

[46] M. Weber, K. Bewilogua, H. Thomsen, R. Wittorf, Surface and Coatings Technology 201 (2006) 1576–1582.

[47] D. Hofmann, S. Kunkel, K. Bewilogua, R. Wittorf, Surface and Coatings Technology 215 (2013) 357–363.

[48] K.-R. Lee, K. Yong Eun, I. Kim, J. Kim, Thin Solid Films 377-378 (2000) 261–268.

[49] J. Robertson, Materials Science and Engineering: R: Reports 37 (2002) 129–281.

[50] E. Broitman, L. Hultman, in: S. Hashmi, G.F. Batalha, C.J. van Tyne, B.S. Yilbas (Eds.),

Die approbierte gedruckte Originalversion dieser Diplomarbeit ist an der TU Wien Bibliothek verfügbar
The approved original version of this thesis is available in print at TU Wien Bibliothek.
TU Bibliothek Your knowledge hub WIEN

Comprehensive materials processing, Elsevier, Oxford, Walltham, MA, 2014, pp. 389–412.

[51] L. Zauner, P. Ertelthaler, T. Wojcik, H. Bolvardi, S. Kolozsvári, P.H. Mayrhofer, H. Riedl, Surface and Coatings Technology 382 (2020) 125007.

[52] R. Ganesan, D.G. McCulloch, N.A. Marks, M.D. Tucker, J.G. Partridge, M.M.M. Bilek, D.R. McKenzie, J. Phys. D: Appl. Phys. 48 (2015) 442001.

[53] J.A. Santiago, I. Fernández-Martínez, J.C. Sánchez-López, T.C. Rojas, A. Wennberg, V. Bellido-González, J.M. Molina-Aldareguia, M.A. Monclús, R. González-Arrabal, Surface and Coatings Technology 382 (2020) 124899.

[54] DIN 28403:1986-09, Vakuumtechnik; Schnellverbindungen; Kleinflansch-Verbindungen, Beuth Verlag GmbH, Berlin, 1986.

[55] DIN 28404:1986-10, Vakuumtechnik; Flansche; Maße, Beuth Verlag GmbH, Berlin, 1986.

[56] ISO 3669 Vacuum technology - Dimensions of knife-edge flanges, Beuth Verlag GmbH, Berlin, 2020.

[57] P. Couturier, IFAC Proceedings Volumes 39 (2006) 167–172.

[58] DIN 1343:1990-01, Referenzzustand, Normzustand, Normvolumen; Begriffe und Werte, Beuth Verlag GmbH, Berlin, 1990.

[59] DIN EN ISO 10156:2017-12, Gasflaschen - Gase und Gasgemische - Bestimmung der Brennbarkeit und des Oxidationsvermögens zur Auswahl von Ventilausgängen, Beuth Verlag GmbH, Berlin, 2017.

[60] E. Brandes, W. Möller, Brennbare Flüssigkeiten und Gase, Sicherheitstechnische Kenngrößen / [PTB; BAM] ; Bd. 1, Wirtschaftsverl. NW, Bremerhaven, 2003.

[61] DIN EN 1127-1:2019-10, Explosionsfähige Atmosphären - Explosionsschutz - Teil 1: Grundlagen und Methodik, Beuth Verlag GmbH, Berlin, 2019.

[62] IEC 62061, Sicherheit von Maschinen - Funktionale Sicherheit sicherheitsbezogener elektrischer, elektronischer und programmierbarer elektronischer Steuerungssysteme, Beuth Verlag GmbH, Berlin, 2016.

Die approbierte gedruckte Originalversion dieser Diplomarbeit ist an der TU Wien Bibliothek verfügbar
The approved original version of this thesis is available in print at TU Wien Bibliothek.
TU WIEN Bibliothek Your knowledge hub

A. Objects

Table A.1: Devices, components, sensors and valves for the operation of the PVD system.

	Object Nr.	Name	Producer
Cooling water	1102BZ01	Flow & temperature sensor water inlet	SMC
	1102BZ11	Flow & temperature sensor, water outlet cathode	SMC
	1102BZ21	Flow & temperature sensor, water outlet heater and turbopump	SMC
	1102PH01	Display unit: flow rate, temperature, water inlet	SMC
	1102PH11	Display unit: flow rate, temperature, water outlet cathode	SMC
	1102PH21	Display unit: flow rate, temperature, water outlet heater and turbopump	SMC
Heating	1143EB01	Chamber heating	Horst
	1162BT01	Thermocouple substrate heating	Therma
	1162EB01.1	Heater lamp	Osram
	1162EB01.2	Heater lamp	Osram
	1162KK01	Sample heating controller	Jumo
	1162TA01	Power electronics sample heating	FG-Elektr.
	1162TF01	Substrate heating temperature transmitter	RS
Process	1101A01	Valve terminal	SMC
	1104KK01	Shutter magnetron 1	SMC
	1104KK02	Shutter magnetron 2	SMC
	1104KK03	Reserve valve 1	-
	1104KK04	Reserve valve 2	-
	1111PC01	Industrial PC	Spectra
	1111TA01	DC generator cathode 1	ADL
	1111TA02	DC generator cathode 2	ADL
	1111TA03	DC generator BIAS	ADL
	1111TA04	HiPIMS generator, 2 channels	Melec
	1111TA05	Diode module	Melec
	1143BP11	Vacuum gauge process pressure CMR	Pfeiffer Vacuum
	1143KK31	Sealing gas valve turbopump	SMC
Process gas	1103BF11	Acetylene mass flow controller	MKS
	1103BF21	Nitrogen mass flow controller	MKS
	1103BF31	Argon mass flow controller	MKS
	1103BF41	Flow switch gas dilution	IFM
	1103BG13.1	Position indicator valve 1 oxygen/acetylene	Swagelok
	1103BG13.2	Position indicator valve 2 oxygen/acetylene	Swagelok
	1103KK01	Gas flow control unit	Jevatec
	1103KK11.1	Stop valve 1 oxygen/acetylene	Swagelok
	1103KK11.2	Stop valve 2 oxygen/acetylene	Swagelok
	1103KK21	Stop valve nitrogen	Swagelok
	1103KK31	Stop valve argon	Swagelok

Die approbierte gedruckte Originalversion dieser Diplomarbeit ist an der TU Wien Bibliothek verfügbar
The approved original version of this thesis is available in print at TU Wien Bibliothek.
TU WIEN Bibliothek Your knowledge hub

Continued Table A.1

	Object Nr.	Name	Producer
Safety	1103KK12.1	Solenoid valve 1 oxygen/acetylene	SMC
	1103KK12.2	Solenoid valve 2 oxygen/acetylene	SMC
	1121BG01	Door safety switch machine frame with lock	Bernstein
	1121BG02	Door switch main chamber	Bernstein
	1131BG01	Door switch load-lock	Bernstein
	1141BP01.1	Vacuum switch	Inficon
	1141BP01.2	Vacuum switch	Inficon
	1141BP02	Baratron switch	MKS
	1143BP21	Monitoring foreline valve	Pfeiffer Vacuum
Substr	1161MA01	24V DC motor substrate rotation	Micromotors
	1161RA01	10-kΩ potentiometer	Conrad
	1161TA01	DC motor speed controller	FG-Elektr.
Vacuum	1123MA01	Vacuum backing pump	Pfeiffer Vacuum
	1132BP01	Load-lock vacuum gauge atm-HV	Pfeiffer Vacuum
	1132KK01	Load-lock valve	Pfeiffer Vacuum
	1143BP01	Main chamber vacuum gauge UHV	Pfeiffer Vacuum
	1143BP02	Main chamber vacuum gauge atm-HV	Pfeiffer Vacuum
	1143BP03	Main chamber vacuum gauge atm-HV 2	Pfeiffer Vacuum
	1143KK11	Baratron valve	Pfeiffer Vacuum
	1143KK21	Foreline valve	Pfeiffer Vacuum
	1143MA01	Vacuum turbopump	Pfeiffer Vacuum
	1143PH01	Vacuum gauge display and control unit	Pfeiffer Vacuum
	1143TA01	Control unit vacuum turbo pump	Pfeiffer Vacuum

Die approbierte gedruckte Originalversion dieser Diplomarbeit ist an der TU Wien Bibliothek verfügbar
The approved original version of this thesis is available in print at TU Wien Bibliothek.
TU WIEN Bibliothek Your knowledge hub

B. Temperature Calibration Curves

This chapter shows the recorded temperature curves and calibration curves of the substrate heater. For all tests two thermocouples were mounted on the sample holder. The cooling water temperature was 16 °C and the base pressure below 10^{-5} mbar in all tests, performed in the end of July 2019. It is recommended to repeat the tests annually. Figure B.1 shows the temperature curves at maximum power. The cooling rate is very low, the cooldown takes a minimum of 1.5 hours. The maximum T is about 640 °C. T is below 100 °C when the heater indicates 60 °C. Figure B.2 shows a T-Curve with different set points. There is always an overshoot of maximum 30 °C and T is stable after about 20 minutes. The calibration curve is shown in Figure B.3 and the recommended set points in 50 °C steps are given according the polynomial trend line.

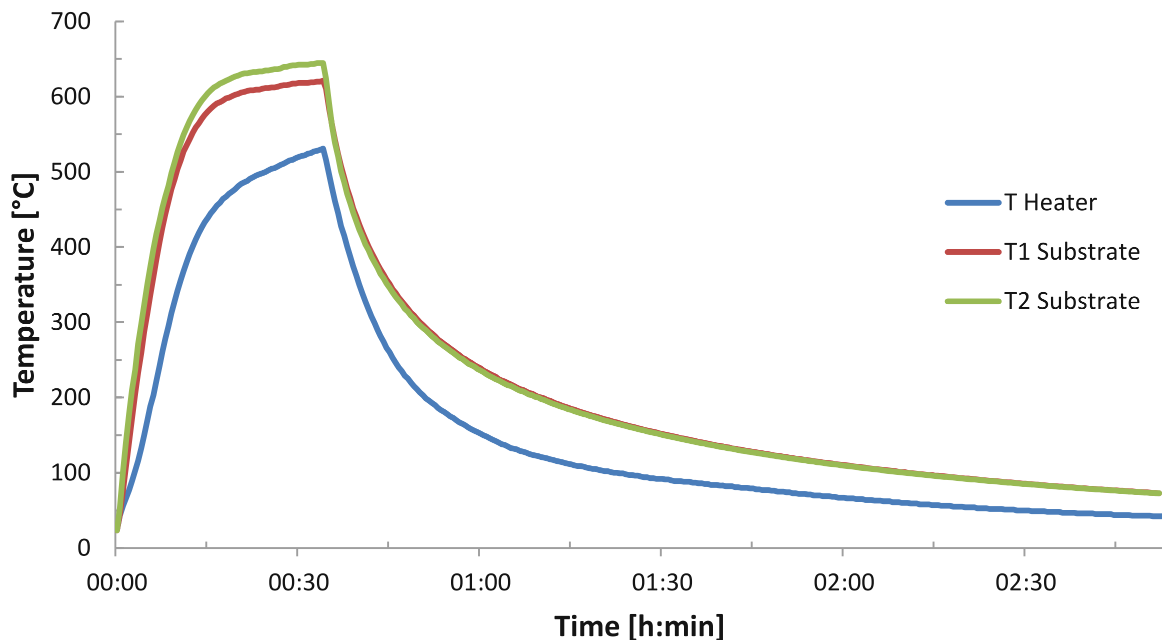

Fig. B.1: Temperature curve at maximum power.

Die approbierte gedruckte Originalversion dieser Diplomarbeit ist an der TU Wien Bibliothek verfügbar
The approved original version of this thesis is available in print at TU Wien Bibliothek.
TU WIEN Bibliothek Your knowledge hub

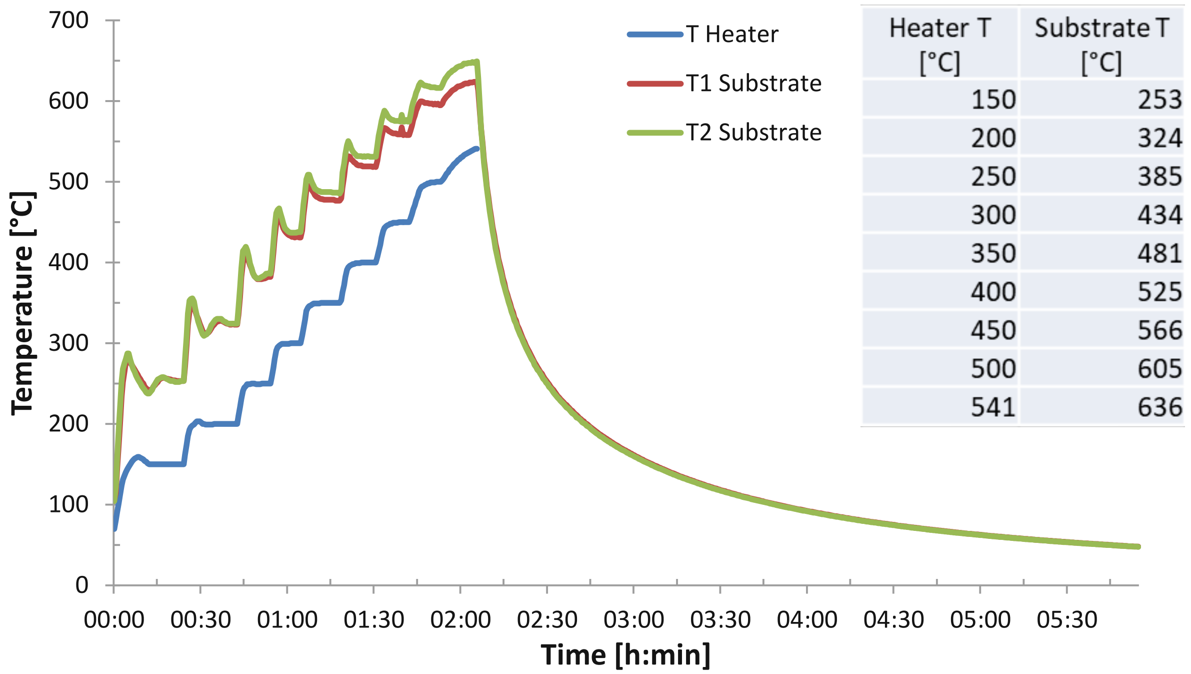

Heater T [°C]	Substrate T [°C]
150	253
200	324
250	385
300	434
350	481
400	525
450	566
500	605
541	636

Fig. B.2: Temperature curve with set points in 50 °C steps.

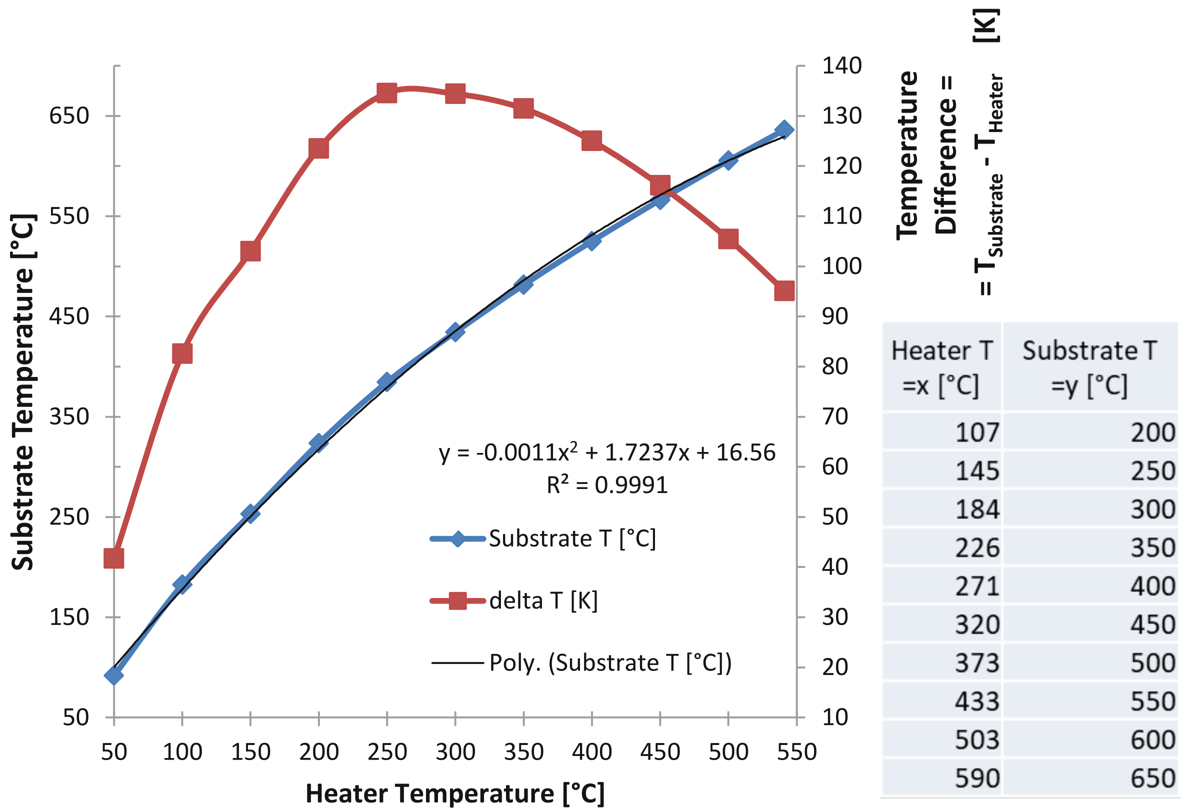

Heater T =x [°C]	Substrate T =y [°C]
107	200
145	250
184	300
226	350
271	400
320	450
373	500
433	550
503	600
590	650

Fig. B.3: Calibration curve of the substrate heater and recommended heater set points

Die approbierte gedruckte Originalversion dieser Diplomarbeit ist an der TU Wien Bibliothek verfügbar
The approved original version of this thesis is available in print at TU Wien Bibliothek.
TU WIEN Bibliothek Your knowledge hub

C. Figure

Fig.C.1: Frida built up.

Die approbierte gedruckte Originalversion dieser Diplomarbeit ist an der TU Wien Bibliothek verfügbar
The approved original version of this thesis is available in print at TU Wien Bibliothek.
TU WIEN Bibliothek Your knowledge hub